Project Title: **Center for Radiative Shock Hydrodynamics**
Technical Report and Renewal Proposal
DOE Cooperative Agreement Number DE-FC52-08NA28616

Date: May 15, 2011
Period Covered: April 16, 2010 through April 14, 2011

Project Director:
R Paul Drake, Atmospheric, Oceanic and Space Sciences,
University of Michigan

Co-Principal Investigators:
Marvin L. Adams, Nuclear Engineering, Texas A & M University
James P. Holloway, Nuclear Engineering and Radiological Sciences, University of Michigan
Kenneth G. Powell, Aerospace Engineering, University of Michigan
Quentin F. Stout, Computer Science and Engineering, University of Michigan

Co-Investigators, University of Michigan:
Natasha Andronova, Atmospheric, Oceanic and Space Sciences
Krzysztof J. Fidkowski, Aerospace Engineering
Bruce Fryxell, Atmospheric, Oceanic and Space Sciences
Tamas I. Gombosi, Atmospheric, Oceanic and Space Sciences
Eric Johnsen, Mechanical Engineering and Applied Mechanics
Smadar Karni, Mathematics
Carolyn C. Kuranz, Atmospheric, Oceanic and Space Sciences
Edward W. Larsen, Nuclear Engineering and Radiological Sciences
William R. Martin, Nuclear Engineering and Radiological Sciences
Eric Myra, Atmospheric, Oceanic and Space Sciences
Vijayan Nair, Statistics
Philip I. Roe, Aerospace Engineering
Igor Sokolov, Atmospheric, Oceanic and Space Sciences
Katsuyo Thornton, Materials Science and Engineering
Gabor Toth, Atmospheric, Oceanic and Space Sciences
Bartholomeus van der Holst, Atmospheric, Oceanic and Space Sciences
Bram van Leer, Aerospace Engineering
Co-Investigators, Texas A & M University:
Nancy Amato, Computer Science
Bani Mallick, Statistics
Ryan G. McClarren, Nuclear Engineering
James E. Morel, Nuclear Engineering
Lawrence Rauchwerger, Computer Science
Co-Investigator, Simon Frazier University:
Derek Bingham, Statistics

Executive Summary

The goal of the Center for Radiative Shock Hydrodynamics (CRASH) is to develop and demonstrate methods for the Assessment of Predictive Capability (APC) of complex computer simulations, by working with simulations of radiative shock experiments performed on high-energy laser systems. The radiative shocks are driven in xenon gas by a Be plasma accelerated to > 150 km/s by laser ablation. The simulations are based on adding capability to two codes: the Block-Adaptive Tree, Solar-wind Roe-type Upwind Scheme (BATSRUS) code used extensively in space weather modeling by the University of Michigan (UM), and the Parallel Deterministic Transport (PDT) code developed initially for neutron transport calculations on massively parallel computers by Texas A&M University (TAMU).

Since being funded on April 15, 2008, CRASH has released versions of a modified BATSRUS code through 2.2, and has used it for initial studies to gain experience with the end-to-end process of uncertainty quantification (UQ) and APC. Our first assessment of predictive capability to employ calibration, using one-dimensional simulations, is discussed in this report. This experience has prepared us move to the more complete and realistic studies now underway.

We will soon release CRASH 3.0, which will include a laser package in addition to multigroup-diffusion radiation transport, dynamic adaptive mesh refinement, and flux-limited electron heat transport. Our attention has turned primarily to improvements that are needed for more efficient operation to support the many runsets that are underway for UQ, to more extensive code validation, and to radiation transport assessments by comparison with results of the higher fidelity PDT model.

We have also now conducted several experiments chosen for the value to APC. These include experiments aimed at quantifying experimental variability, at calibrating the initialization of our models, at providing data for use in the predictive study with calibration, and at observing the early-time evolution of the radiative shock.

Education of graduate students is an important aspect of CRASH. At present, we have 30 graduate students and 3 recent graduates whose research is, was, or will be supported at least in part by the center. These students are working on all aspects of the project, including experiments, fluid dynamics modeling, radiation transport methods, uncertainty quantification, and APC methods.

Our progress in all the above areas is discussed in the present report. The third annual review of the center was held in October 2010. Our plans for the next year are strongly responsive to the recommendations of the review team. Specific details are included in the present report and especially in our plans for the next year.

Table of Contents

Executive Summary 2
Year 3 Report 4
I. Summary Overview 4
II. Assessment of Predictive Capability (APC) 9
Integrated Metrics 9
Predictive Study for Shock Location at 20 and 26 ns 11
Year 4 Uncertainty Quantification Plans 14
III. Code development, verification, and testing 16
Limiting the Electron Heat Flux 18
Decoupled Semi-Implicit Update 18
Laser Energy Deposition Package for CRASH 19
Parallel Deterministic Transport (PDT) 22
Difference between transport and diffusion 25
Iterative algorithms 26
Year 4 Transport Plans 27
IV. Experiments 28
V. CRASH Applications 31
Non-radiative Variations on the CRASH Experiment 31
X-ray driven initialization for studying shock structure 34
Ablation of low-Z walls by x-ray ablation 35
A CRASH-like problem initiated with x-radiation 36
V. Educational Status and Plans 39
VI. Graduate Student Research 40
Computational and Statistical Students: 40
Experimental Students 45
VII. References 47

Year 3 Report

The present section is our technical report. It summarizes the work we have accomplished from April 2010 through January 2011 and connects with our plans for the next year.

I. Summary Overview

The overarching goal of the CRASH project is to use scientific methods to assess and to improve the predictive capability of a simulation code, based on a combination of physical and statistical analysis and experimental data. The specific focus of the project is radiative shocks, which develop when shock waves become so fast and hot that the radiation from the shocked matter dominates the energy transport. This in turn leads to changes in the shock structure. Radiative shocks are challenging to simulate, as they include phenomena on a range of spatial and temporal scales and involve two types of nonlinear physics – hydrodynamics and radiation transport. Even so, the range of physics involved is narrow enough that one can seek to model all of it with sufficient fidelity to reproduce the data.

The CRASH project builds upon the basic physical system shown in Figure 1. Ten (0.35 μm wavelength) laser beams from the Omega laser[1] are incident on a 20-μm thick Be disk, at an irradiance of ~ 7 x 10^{14} W/cm^2 for 1 ns. This shocks the Be and then accelerates the resulting plasma to > 100 km/s. The leading edge of this plasma drives a shock into Xe gas at 1.1 atm pressure with an initial velocity of ~ 200 km/s. This produces the observable structures shown schematically in Figure 1b and by a radiograph in Figure 1c. The radiation from the shocked Xe preheats the unshocked Xe. It also ablates the shock-tube wall, producing a "wall shock" that drives the Xe gas inward. Where this wall shock meets the primary shock, the shock-shock interaction produces a noticeable deflection of the dense Xe flow (dark in the radiograph). The Xe that flows through both the wall shock and the oblique portion of the primary shock ends up with higher velocity and forms the material described as entrained Xe. On a finer scale than is seen in the radiograph, the shocked Xe ions, which are initially heated to hundreds of eV, cool rapidly as they ionize and heat the

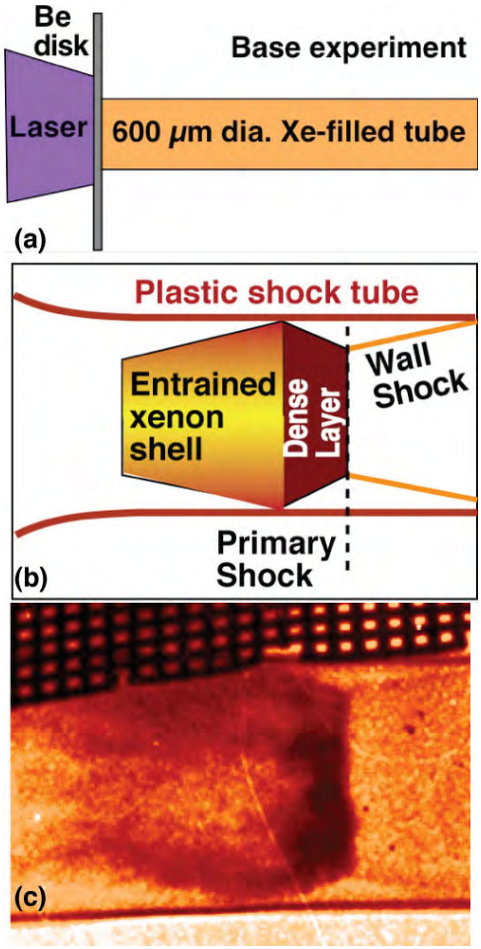

Figure 1. (a) Schematic of a radiative shock experiment. (b) Schematic of features in radiograph. (c) Radiograph. The structure in the dense Xe may be due to a Vishniac-type instability.

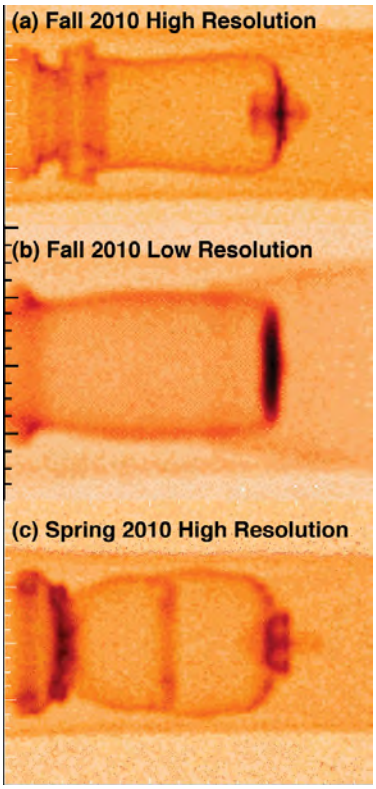

Figure 2. Radiographs at 13 ns from CRASH simulations illustrating the variation in simulated morphology (a) 2400 x 240 CRASH 2.1 RZ. (b) 640 x 64 effective CRASH 2.1 RZ. (c) 2400 x 240 CRASH 2.0 RZ.

electrons, and the heated electrons radiate most of their energy away. In response, the shocked Xe layer, which is optically very thick, becomes several times denser. The resulting final temperature in the shocked matter and characteristic radiation temperature is about 40 eV. In contrast, the radiation mean free path in the unshocked Xe is much longer and the radiation transport is not diffusive there.

The radiograph in Figure 1 shows fundamentally where the dense Xe is. Our goal is to predict the area where dense Xe exists and selected moments of the distribution of such locations, in addition to the shock location. We choose these moments, and where they are evaluated relative to the tube wall and shock location, so that they are sensitive to the accuracy with which our simulation evaluates physical aspects of the system, such as the thickness of the dense Xe layer or the inward displacement of this layer by the wall shock. We had originally planned to predict the location and properties of various features in the radiograph, such as the triple point where the three shocks meet. However, these features proved to vary significantly in both experimental data and simulation output (see Figures 2 and 3), and so were not robust enough to be the focus of a predictive study, and especially one requiring automated analysis of images. This led us to develop our present approach, suggested in part by one of our TST members.

While we were developing our revised approach to analyzing radiographs for uncertainty quantification, we carried though our first predictive study involving calibration, using one-dimensional simulations to predict shock location. We used the data measuring shock breakout from the Be disk obtained during Year 2 to calibrate the physical inputs to the simulation and then used the data from radiographs obtained at 13 to 16 ns to estimate the discrepancy for predicting shock location at 20 and 26 ns. The predicted values were consistent with the observations, although the predicted uncertainties were quite large. This process prepared us for the predictive studies we are now

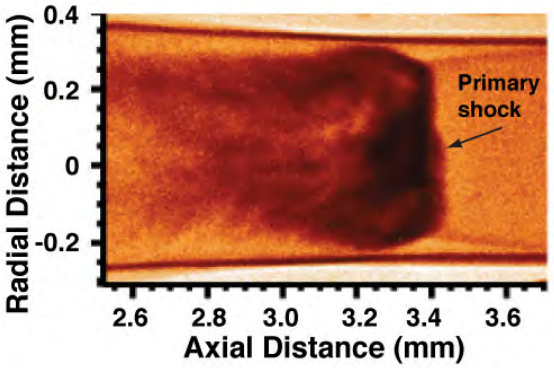

Figure 3. Experimental radiograph at 26 ns. Note the differences in structure near the shock tube walls both by comparison with Figure 2 and between the top and bottom of this image.

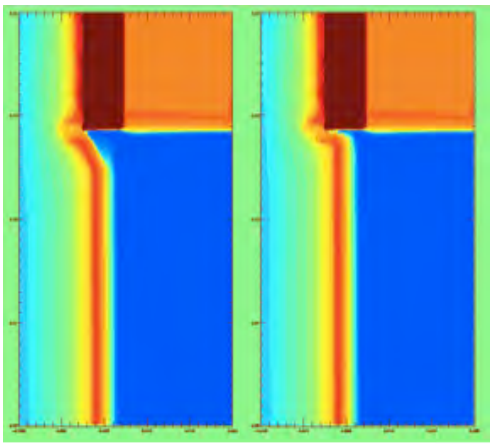

Figure 4. Effect of rezoner settings on Hyades simulation outputs. Log density is shown on an RZ plot. The rezoner is automatically adjusting a specified number of zones near the intersection of Be, Xe, and gold on the upper left. The only difference in these runs is that 6 zones are adjusted for the left case while 3 are for the right.

undertaking using 2D and 3D simulations. We are now typically queue-limited in running simulations on Hera at LLNL and Lobo at LANL, and also are running regularly on several hundred cores on FLUX at Michigan. From November through January we completed nearly 300 2D runs and nearly 600 1D runs in support of the UQ run plan described below. During the year we published three papers based on our first UQ study the previous year.[2-4] We also submitted a conference paper reporting a UQ study using the Year 2 data.[5]

A rate-limiting element for our predictive-science studies has been the Hyades code, a serial, Lagrangian, rad-hydro code that we have used to model the laser-energy deposition phase of the experiment. With the arrival of a rezoner for this code, we proved able to accomplish the sets of order 100 runs needed for our UQ studies. In particular, we completed during 2010 a run set that we are using to initiate the current multi-dimensional UQ runs for CRASH. However, we encountered a number of issues that led us to decide that it was necessary for us to implement a laser package in CRASH. Figures 4 and 5 illustrate two of the issues that support this decision. Figure 4 illustrates that rezoning impacts the region where Be, Xe, and Au interact, which is where the wall shock-primary shock interactions will later become important. It is worth noting that manual rezoning will produce similar variations though in a less controlled and less quantifiable fashion. Figure 5 shows that running the same physical problem, driven by thermal radiation, produces very different results when Hyades is used for the first ns than it does when only CRASH is used throughout. We do not know why this occurs; it might reflect some inadequacy in our mapping of the parameters between codes, although we have examined this closely, or the lack of conservation of vorticity in Hyades, or something else. We believe that Hyades is a very

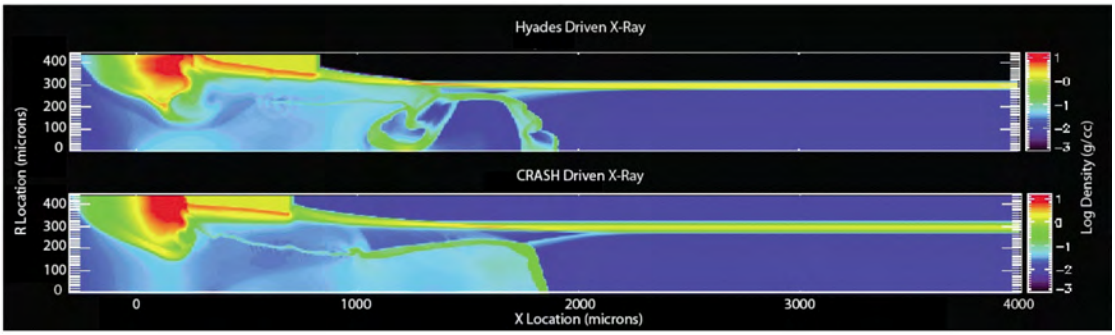

Figure 5. Results from two simulations that should give identical results. In both cases, a 167 eV thermal x-ray flux irradiates a 34 μm thick Be disk for 1 ns and results are shown at 13 ns. Top: run in Hyades for 1 ns then CRASH. Bottom: run only in CRASH.

useful code for experiment design and for other things Lagrangian codes are generally used for. However, doing UQ studies of systems that generate substantial vorticity, as we need to do, is not an area of strength for this code.

Our work on our primary code, an adaptation of the BATSRUS space-weather code that we label CRASH, has undergone a transition in this past year. Aside from the laser package, we have all the physics in the code that we believe is needed for the CRASH project. In the past year we have added flux limiting to the electron heat transport model, but otherwise have not increased its nominal physics content. Instead, the work on the code has evolved to address the needs of doing large numbers of simulations on multiple platforms. In this vein, we have improved the parallel I/O, have made progress on the multigroup preconditioner, and have begun adapting the code to enable it to work with EOS or opacity tables from various sources. This last is particularly important for handling the wide variety of materials needed in diverse validation problems and other applications. This state of affairs has made it timely to submit a paper on the code itself, and we have done so.[6] In addition, as users have identified problems, we have supported resolution of those issues and when necessary the repair of bugs in the code. The most significant such issue was the discovery that one of our two level-set methods for identifying material in each cell was much better than the other in separately conserving the mass in each species. Adopting the better method significantly improved the general similarity of the simulated output to the experiments. In a parallel effort in support of the broad UQ effort, we made significant progress in implementing adjoint methods within the hydrodynamic part of the calculation.

We intend to obtain our highest-fidelity simulations of the experiment by coupling the hydrodynamic solver in CRASH with radiation transport using the PDT code of TAMU. This year we greatly improved the parallel scaling of PDT, so that this coupling would be practical. In addition, continued standard test problems show that PDT remains capable of highly accurate radiation transport solutions. For the standard CRASH problem, we are proceeding to use PDT, in coordination with CRASH, to assess the magnitude of the errors in energy transport produced by the multigroup diffusion model in CRASH. This will provide important information in setting project priorities. Unfortunately, we have been prevented for making progress toward integrating the two codes by a ruling from DOE that such a combined code would be considered Unclassified Controlled Nuclear Information (UCNI), reflecting the content of a regulation that is at best badly outdated. Our Review Team report emphasized the need for DOE to address this. We hopefully await the outcome.

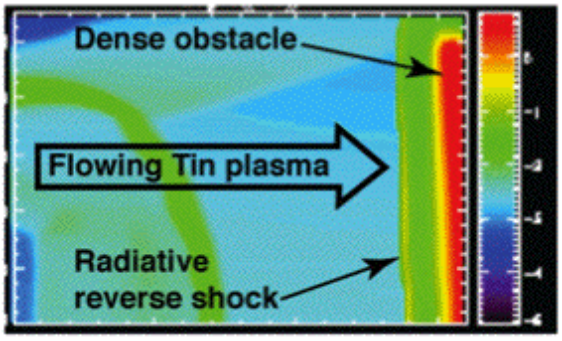

Figure 6. Log density plot from part of a CRASH simulation of radiative reverse shock experiment. CRASH was used to assess design options.

For numerous reasons, including the identification of bugs, it is useful to apply the CRASH code to a range of physical problems. We first developed the x-ray driven case, discussed above with reference to Figure 5, in the context of modeling experiments at the National Ignition Facility. We used this capability this year to examine the structure produced by ablation from shock-tube walls, as part of an effort to assess the impact of limited resolution in multidimensional calculations with CRASH and Hyades. During this past year, we also used CRASH initialized by Hyades to model a new experiment to produce a radiative reverse shock. This would be a first in the laboratory and is relevant to cataclysmic variable stars. Figure 6 shows output from one of these simulations. We used CRASH to assess details of the experimental geometry in two dimensions. CRASH correctly predicted the timing of the collision producing the reverse shock. We also used CRASH in 3D to examine purely hydrodynamic experiments with nozzles, as is described below, and to simulate systems exhibiting hydrodynamic instability.

In support of the above efforts, we have pursued several calculations in the fundamental physics that underlies the CRASH system. We published papers on the essential behavior of the CRASH radiative shock[7] and also on the radiation transport in that type of system.[8] We developed a theory of the structure produced when x-rays irradiate the low-Z walls of a shock tube, and are working on simulations that will support a publication on this physics. We are supporting two of the world's experts in opacity (Marcel Klapisch and Michel Bousquet) to provide us with opacities from super-transition arrays (STA) models of materials that are relevant to CRASH and to help us address non-LTE effects. We are also pursuing the comparison of discrete ordinates and flux-limited diffusion results for our class of problems, as mentioned above.

Our experiments continue to provide data needed by our predictive capability studies. We have now published (or submitted) four papers[9-12] on CRASH radiographic studies of our basic radiative shocks, one of which includes a Bayesian analysis of uncertainty that would not have occurred without the intellectual mixing produced by this project. Another of these publications discusses the late-time radiographs obtained this year and mentioned above. We have analyzed the shock breakout experiments of Year 2, which has led to one publication in submission[5] and one in preparation. Our Year 3 experiments, chosen to have the maximum impact on assessing and improving our predictive capability, are focused on the shock behavior at very early times and are discussed below.

An additional important aspect of the project is education and training. Education of graduate students is an important aspect of CRASH. At present, we have 30 graduate students whose research is, was, or will be supported at least in part by the Center, in addition to 3 recent graduates. Their research activities, and those of our three recent graduates, are described in a section below. These students are working on all aspects of the project, including experiments, fluid dynamics modeling, radiation transport methods, uncertainty quantification and assessment of predictive capabilities methods. Many of these students, and students from other research projects, attended the courses in predictive science that we offered. In addition, several of these students, and several from outside the CRASH project, are enrolled in the Scientific Computing certificate program at Michigan. This program requires several courses in numerical methods, several

courses in computer science, in addition to the requirements for the PhD in the student's home department. Some of the CRASH students enrolled in the certificate program are pursuing the Predictive Science track of the Scientific Computing certificate. This track requires the new course "Uncertainty Quantification for Large-Scale Engineering Simulations, offered by CRASH faculty starting in Winter 2010. A similar course was developed and taught at Texas A&M University in Fall 2009.

In the following several subsections, we provide an expanded discussion of topics mentioned in the present section.

II. Assessment of Predictive Capability (APC)

Our overarching project goal is to develop a simulator – the CRASH code – that can predict radiative shock behavior in an unexplored region of the experimental input space – the elliptical tube – after being assessed in a different region of input space that has been explored by experiments. Our unique intended contribution is to be the first academic team to use statistical assessment of predictive capability to systematically guide improvements in simulations and improvement in experiments so as to produce new predictions of improved accuracy, and to demonstrate this improvement by experiment. CRASH employs both sensitivity studies, to assess which aspects of the physical system are important and which are not, and predictive model construction, to assess the probability distribution functions of both physical parameters and experimental outputs. This year saw two key developments, described here. The first was the realization that the use of integrated metrics was essential to the project, and the development of such metrics. The second was our first end-to-end predictive study that included calibration.

Integrated Metrics

Our predictive work is predicated on extracting a few scalar parameters from both experimental data (in the form of radiographs) and from simulation data (also in the form of simulated radiographs). Because there is considerable variability in the structures in our system, both in physical experiments and in simulations, we have developed a robust set of integrated metrics that are less sensitive to interface details. The integrated metrics provide information about the fundamental information given by the radiographs: how much dense xenon there is, where is it located, and how much is flowing near the edges. Within a fixed window (shown in Figure 7) we extract a set of metrics:

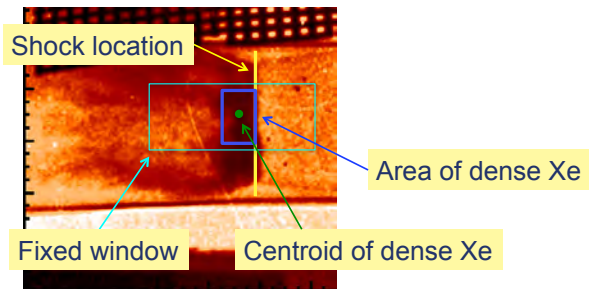

Figure 7. Illustration of some of the integrated metrics adopted this year.

1. the (projected) area of dense Xe, defined as the area where the optical depth is larger than a given threshold times the optical depth of the unshocked Xe
2. the axial centroid of the dense Xe
3. the radial rms of the dense Xe over a window extended to the tube walls (not shown in the figure)
4. the breakpoints of a piecewise constant fit with 4 to 7 segments (the first such breakpoint is diagnostic of the shock location)

Shown in Figure 8 are the simulated radiographs from the first 64 runs of UQ Run Set 6, each paired with an image showing the location of pixels which exceed a threshold value - a multiple of the absorption of the upstream xenon. In the images below, the pixels-above-threshold (PATs) are shown in white. The window extends from 1.3 mm to 2.5 mm in the axial direction and 0.1 mm from the centerline radially. The area of PATs is calculated by using the known pixel size in microns. The axial centroid is then calculated by: $\sum n_x * x/N$ where n_x is the number of PAT at a location x and N is the total PAT in the window. The process of finding PATs is repeated over a window spanning the entire tube diameter to calculate the radial variance of the PATs.

We use a separate program to fit a plot of the optical depth with a piecewise constant function and return the breakpoints of the best L_1 (or L_2) fit. The breakpoints give information about the shock location as well and thickness of the shocked layer can be extracted using this information. These fits are done using the same axial window as the

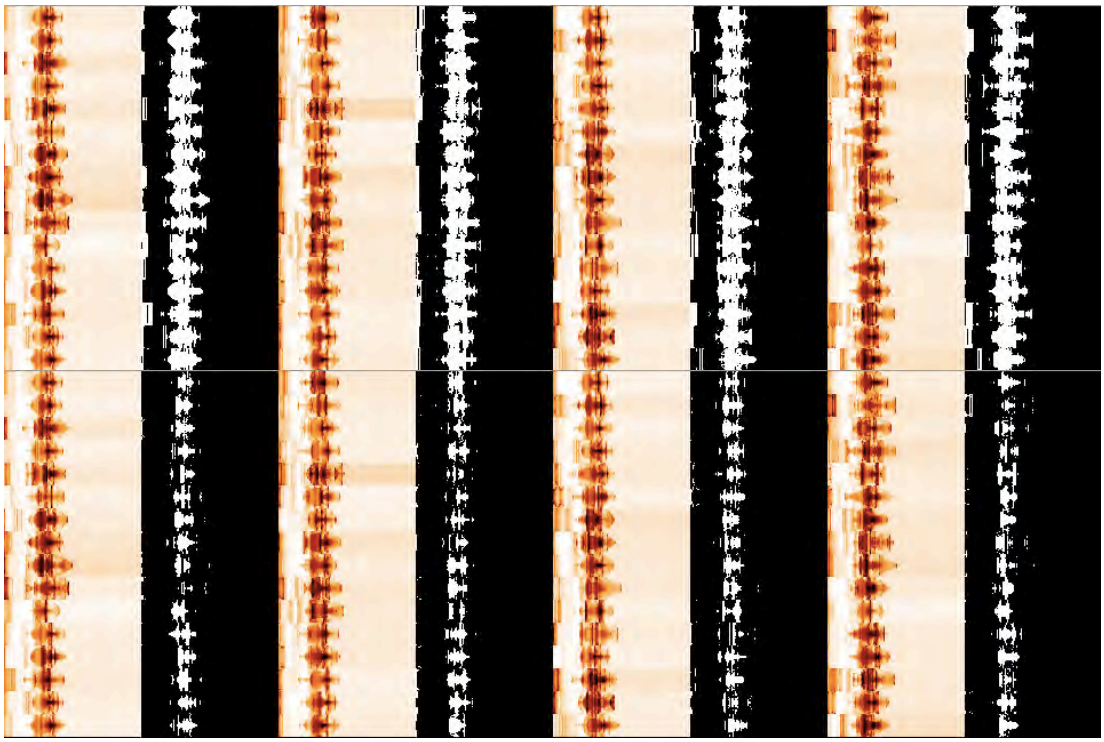

Figure 8. Selectred near-axis regions from simulated radiographs from the first 64 runs of UQ Run Set 6 are shown as colored images. The corresponding white images show the pixels-above-threshold (PATs), where the threshold is a multiple of the absorption of the upstream xenon. The top image has a threshold of 2x and the bottom has a threshold of 4x.

area and centroid metrics. Robustness of the piecewise fit is established by varying the number of segments in the fit.

Predictive Study for Shock Location at 20 and 26 ns

The CRASH experiment creates a high energy density radiative shock in a Xe-filled tube, with a shock velocity on the order of 100 km/s. The shock is first created in a Be metal disk 20 microns thick by a 1 ns laser pulse of 360 J. The shock breaks out of this disk some 400 ps after the initiation of the laser pulse, and continues down the Xe-filled tube, compressing and heating the Xe sufficiently to radiate, and this radiation in turn preheats the Xe ahead of the shock and ablates the plastic wall of the tube, creating additional radial shocks traveling inwards from the wall. To predict the location of the primary shock we use two radiative hydrodynamics codes, Hyades and CRASH. Hyades models the laser-plasma interaction and can predict the shock breakout time and the state of the system at 1.1 ns after the initiation of the laser pulse. The CRASH code, when initialized with this state at 1.1 ns, can predict the shock location at later times when shock location can also be observed in experiments at observation times from 13 to 26 ns.

Our general interest is in using the simulation tools together with experiments conducted in one region of input space, to make predictions in a new region of input space in which no prior experiments have been made. We are generally interested in extrapolation from one region of input space to another, with this extrapolation accomplished by a simulation code that contains the necessary physics. In particular, we have two data sets on which to base predictions: shock break time data, and shock location data at 13, 14 and 16 ns, and wish to predict shock locations at 20 and 26 ns (which are then compared

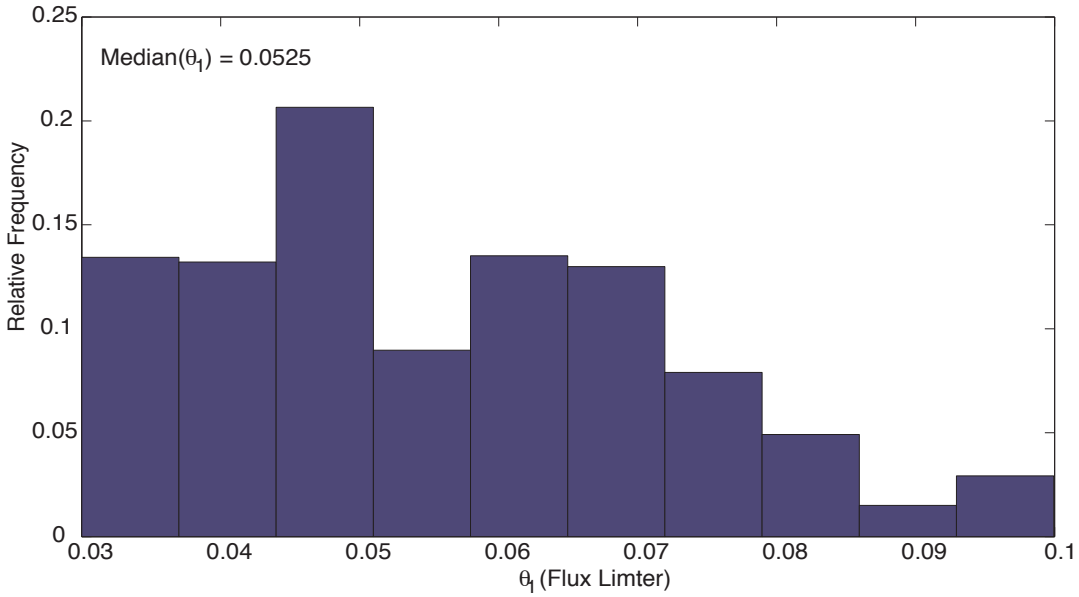

Figure 9: Posterior distribution for electron flux limiter parameter calibrated using shock breakout times. This is the marginal distribution, but the analysis produces samples from the full joint distribution of calibration parameters.

to subsequent field measurements). We use ***two*** models of the Kennedy-O'Hagen form to combine field measurements with simulations, using one to inform the other, and we interpret the discrepancy in these models in a way that allows us to gain some understanding of model error separately from parameter tuning.

To model shock breakout times we construct a model of the form $t = \eta_{BO}(x,\theta) + \delta_{BO}(x) + \varepsilon_{BO}$ that jointly fits the field measurements, T, of shock breakout time t along with a set of 1024 Hyades simulations over a 6 dimensional input space with 4 experimental variables x and 2 calibration parameters θ. This model provides posterior distributions for various modeling parameters, including a posterior $\pi(\theta|T)$ for the calibration parameters, as well as for the parameters in Gaussian process models of the emulator $\eta_{BO}(x,\theta)$, the discrepancy function $\delta_{BO}(x)$ and the replication error ε_{BO}. A sample of such a posterior for the electron flux limiter parameter (marginalized over the other calibration parameter) appears in Figure 9.

If the discrepancy function is significant compared to measurement uncertainty we would call this process "tuning," but if, as is in our case, the discrepancy is small, then we refer to this as calibration (for shock breakout time). Figure 10 shows a leave-one-out predictions of shock location and of shock breakout time, showing the discrepancy compared to the measurement uncertainty. The discrepancy for shock location is significant, while for breakout time it is insignificant. We therefore can calibrate using the breakout data, and will then use shock location time data from 13 to 16 ns to estimate discrepancy for better understanding of predictions at 20 and 26 ns.

Once we have posterior distributions for calibration parameters we then use the shock location field data (at times of 16 ns and less) along with 1024 simulations of shock locations from CRASH to construct a model of the form $z = \eta_{SL}(x,\vartheta) + \delta_{SL}(x) + \varepsilon_{SL}$, but in this model θ is no longer treated as a calibration parameter, but instead is treated as an experimental parameter and is drawn from the posterior constructed in the previous step

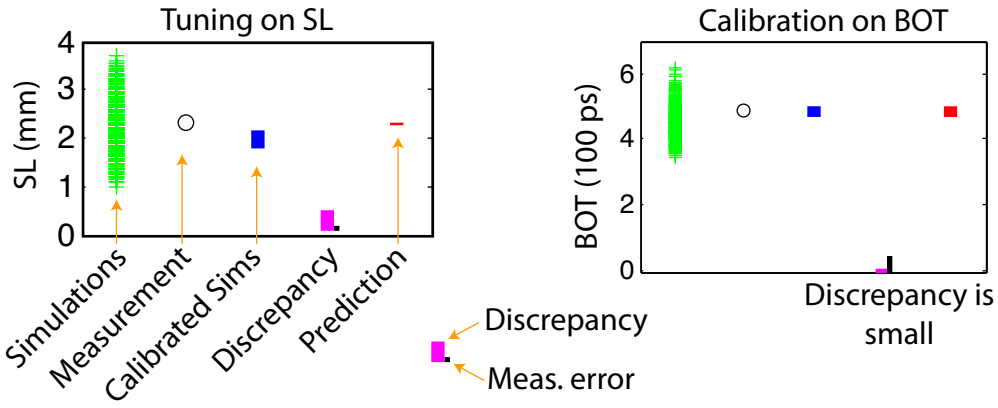

Figure 10: The full set of simulation results (green), a single measurement to predict (open circle), calibrated code predictions (blue), discrepancy (pink) compared to measurement error (black), and finally the prediction of the measurement. All ranges shown are 95% prediction intervals.

$\vartheta \sim \pi(\theta|T)$. The x are also drawn from distributions that represent the understood uncertainties in the experimental parameters. This second model is used to construct the emulator $\eta_{SL}(x,\theta)$ and its discrepancy $\delta_{SL}(x)$, as well as a best estimate of the replication error ε_{SL}, all for shock location. The discrepancy from this model can be studied to understand the defects of the physics model; note that because we have separated calibration from the construction of this discrepancy, the calibration of the θ is not simply masking errors in predicted shock location. The result shows that our model tends to under predict shock location.

Finally we can use $\eta_{SL}(x,\theta)+\delta_{SL}(x)+\varepsilon_{SL}$ to predict shock location at 20 and 26 ns, a region of phase space in which we had simulations but no previous measurements. This produced the results shown in Figure 11. In doing this analysis we can separate the code prediction $\eta_{SL}(x,\theta)$ and the uncertainty due to this prediction (caused by uncertainty in x, θ, and in the Gaussian process modeling parameters) from the uncertainty due to discrepancy $\delta_{SL}(x)$. The uncertainty in discrepancy is of course large, because we are extrapolating the discrepancy to a new region of input space. The uncertainty in the emulator $\eta_{SL}(x,\theta)$ is significantly smaller because there were simulation data in this

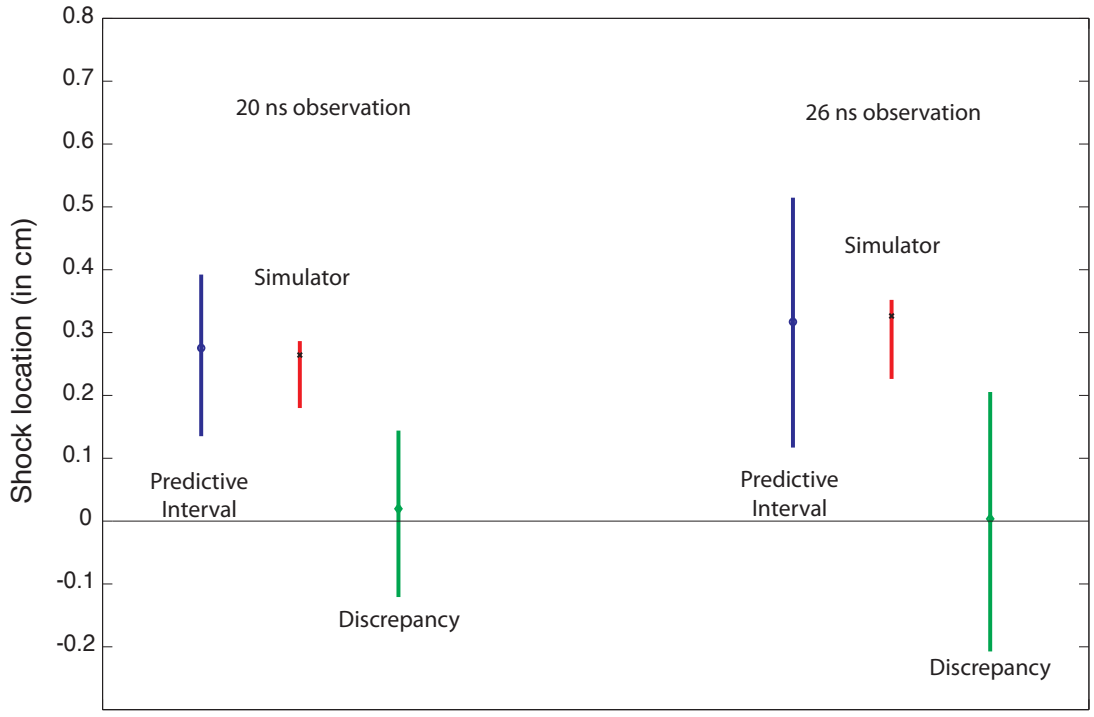

Figure 11. Results of the Kennedy-O'Hagan type analysis with calibration, predicting new observations at 20 ns and 26 ns in advance of knowing the data. The red predictive interval is that due to propagating uncertainties in θ and x through the simulator, and the uncertainties in the emulator $\eta_{SL}(x,\theta)$. In contrast, the blue predictive interval includes the uncertainty due to the discrepancy, which is large because it has been extrapolated from the 13 – 16 ns range out to 20 and 26 ns.

region.

Comparison of the predictions with field measurements at 20 and 26 ns show that even the smaller predictive interval from the emulator alone contains the actual field measurements. The results, shown here as 95% predictive intervals show a median shock location of 2750 microns at 20 ns, and 3200 microns at 26 ns. These compare well with experimental measurements of 2741 ± 70 microns and 3442 ± 30 microns, respectively.

Year 4 Uncertainty Quantification Plans

For year 4 we are developing an approach to constructing calibration models and discrepancy functions using simulations combined from various models. In particular we will combine 1D, 2D and 3D models, grey and multigroup, and potentially different mesh resolutions, along with all previous calibration experiments in order to predict the integrated metrics for a 5th year experiment. To support this we have planned a set of 13 CRASH run sets, of which 3 were completed during previous years to conduct the predictive study described above. The planned full set of runs comprises:

1. 320 runs using 1D Hyades & CRASH
2. 512 runs using 1D Hyades
3. 1024 runs using 1D Hyades & CRASH
4. 104 runs using 2D Hyades and CRASH
5. 1D convergence study (512 runs 1D-Multigroup)
6. 2D convergence study (128 2D-Multigroup)
7. Sensitivity Study (256 runs 2D Grey & Multigroup)
8. 2D nozzle study with large tubes (128 runs 2D-Gray and Multigroup)
9. 3D aspect ratio sensitivity study (256 runs 3D-Gray and Multigroup)
10. Full simulation with 2D-Gray 1024 runs
11. Full simulation with 2D-Multigroup 512 runs
12. Full simulation with 3D-Gray 256 runs
13. Full simulation with 3D-Multigroup 8-16 runs plus 256 medium resolution runs

Different run sets have different purposes in the analysis, and different input spaces. Some of the early runs will be used to assess sensitivity and confirm parameter ranges for numerical convergence. But for the full system simulation we anticipate an 11 dimensional input space of:

1. Electron flux limiter
2. Laser scale factor (to account for laser plasma instabilities)
3. Laser Energy
4. Be Thickness
5. Tube Radius
6. Xe Fill pressure
7. Backlighter fire time
8. Nozzle angle

9. Nozzle length
10. Tube radius (post nozzle)
11. Aspect ratio

Run sets 4, 5, and 6 are on-going or being analyzed.

In addition, in order to assess the importance of radiation transport effects (vs. the workhorse flux-limited diffusion model in CRASH), a static (no hydro) model has been defined that captures some of the radiation transport regimes of the CRASH problem, and this system is being modeled in both CRASH and the PDT transport code. The energy deposition of each model will be compared to assess the importance (or not) of transport effects.

Finally, initial work has begun on assessing the sensitivity of multigroup opacities, as calculated using software developed within the CRASH project, to uncertain parameters (such as ionization potentials) and modeling approximations (such as in models for continuum lowering of potentials).

III. Code development, verification, and testing

As the 2008 review team emphasized, this is where "the rubber meets the road" for the CRASH project. Accordingly, it is the area of activity we initiated most quickly and focused on most strongly after the start of the project. In the first year we released CRASH 1.0, which contained the minimum capabilities to make a crude but physically somewhat reasonable approximation to the experiment. In the second year we implemented those additional physics elements that we considered essential to the success of the CRASH project. This led during the past year (PY3) to the release of CRASH 2.0, and following bug fixes and some functionality improvements CRASH 2.1 and 2.2. Here we summarize the evolution of the code to date.

At the beginning of this project the BATSRUS code contained ideal or resistive magnetohydrodynamics and included

- multispecies and multifluid MHD with ideal EOS
- explicit and fully implicit time discretization
- block adaptive grid in 3D
- Cartesian, cylindrical and spherical grids.

During the first year of the CRASH project we added the following features:

- Non-ideal equation of state for high energy density plasma
- Numerical scheme for strong shocks with non-ideal EOS
- Using 1D or 2D HYADES output to set initial conditions for CRASH
- Tracking and solving for multiple materials
- Reading and interpolating tabular EOS and opacity data
- Gray diffusion radiation transport with flux limiter
- Semi-implicit time discretization (explicit hydro, implicit radiation)
- R-Z geometry in 2D.

The above features were discussed in our Year 1 Annual Report and were used for a year in CRASH 1.0. In the second year we further developed the code to CRASH 2.0 with the following capabilities:

- Equation of state with separate electron temperature
- Calculated multi-group opacities
- Electron energy equation with semi-implicit heat conduction
- Radiative transport with multigroup diffusion
- Synthetic radiographs both for 3D and for R-Z geometry including experimentally appropriate blurring and noise
- Block Adaptive Tree Library (BATL) that provides
    - new capabilities such as 1D and 2D AMR, and
    - significantly more efficient dynamic mesh refinement in 3D.

We also developed the CRASH preprocessors and postprocessors:

- An automatic remap algorithm for HYADES 2D.
- Physics Informed Emulator (PIE) for dimension reduction of the initial conditions in one dimension.
- Feature recognition software to identify shock location, wall shock angle etc. in experimental data and model output.

The third year saw a number of improvements to the code, with emphasis on improved efficiency, robustness and physical fidelity. The primary improvements to the physical fidelity of the code were:

- Addition of electron heat-flux limiting
- Bringing the materials supported by the EOS and opacity package or the code up to the full five materials present in the experiments (Au, Be, Xe, acrylic and polyimide)
- Adding Poisson noise to the synthetic radiograph package to model finite photon count
- Adding blurring to the synthetic radiograph package to model finite apertures

The primary improvements to the efficiency of the code were:

- Implementation of a new block-adaptive tree library (BATL), substantially improving the efficiency of dynamic adaptive meshes, particularly in 1D and 2D
- Implementation of a semi-implicit update for the multigroup diffusion solver, split by energy group to reduce the memory and CPU costs of the diffusion solve.

The primary improvements to the robustness of the code were:

- Basing the hydro update on the full energy, while maintaining the interpolation and slope limiting based on primitive variables
- Making the EOS tables reversible (so that, for example, computing pressure from energy, and then the energy from that pressure, leads back to the original energy)

Ongoing work in code development includes two major thrusts:

1. implementing the ability to read EOS and opacity tables from other sources (e.g. Propaceous) and
2. a laser package built on the block-adaptive structure of the CRASH code.

The ability to read EOS and opacity data from other sources will provide cross-validation ability, and enable quantification of uncertainty arising from material property data. When the laser package is finished, the result will be a powerful tool for cross-validating with HYADES, and for improving the efficiency of runsets by eliminating the hands-on nature of the HYADES initialization.

We have also produced new verification solutions for the coupling of energy between radiation, electrons, and ions, the so-called 3T equations.[8,13] These solutions have used both diffusion and transport models to describe the radiation evolution; diffusion was

used to model the electron transport process. These solutions have impacted work outside CRASH as well, being used in verification exercises at the FLASH center and at Los Alamos National Lab.

The three most fundamental of these improvements – the flux limiting, the semi-implicit update, and the laser package – are described below.

Limiting the Electron Heat Flux

The classical Spitzer-Harm formula shows the collisional electron conductivity to be proportional to $T_e^{5/2}/Z_{eff}^2$, where Z_{eff} is the root mean square ionization of the material (whose average ionization is Z). The collisional model is only valid when the temperature scale length is much larger than the collisional mean free path of the electrons. When the temperature scale length is only a few mean free paths or smaller, this description breaks down. This may for instance happen in laser-irradiated plasmas. In such a case, one could determine the heat flux by solving the Fokker-Planck equation for the electrons, but this is computationally expensive. Instead, we use the standard simplified model to limit the electron heat flux. A free-streaming heat flux F_{FS} can be defined as the thermal energy density in the plasma transported at some characteristic thermal velocity: $F_{FS} = n_e k_B T_e v_{th}$, where $v_{th} = \sqrt{k_B T_e / m_e}$, in which electron density and mass are n_e and m_e, respectively, the electron temperature is T_e, and k_B is the Boltzmann constant.

For practical applications, the maximum heat transport is usually only a fraction of this free-streaming flux: $-(fF_{FS}/|\nabla T_e|)\nabla T_e$, where f is the so-called flux limiter. This heat flux model is the threshold model and is also used in other radhydro packages, such as HYADES.[14] The flux-limited heat flux can now be defined as

$$\mathbf{F} = -\min(C_{SH}, \frac{fF_{FS}}{|\nabla T_e|})\nabla T_e,$$

where C_{SH} is the usual Spitzer-Harm coefficient of heat conduction. The flux limiter is an adjustable input parameter and can be tuned to let the simulated results better fit reality. In our case, it will be set by a Kennedy-O'Hagan calibration process.

Decoupled Semi-Implicit Update

The coupled implicit scheme originally implemented in CRASH requires solution of a large system of equations (G+1 variables per mesh cell, where G is the number of energy groups considered). The preconditioning of such a system can be computationally expensive and requires overall a lot of memory. We therefore also implemented a decoupled implicit scheme that solves each equation independently.

For some applications, the electron temperature does not change much in exchanging energy with the radiation. This is typically so if the electrons have a much larger energy density than the radiation, so that the electron temperature changes little due to interaction with the radiation in a single time step. In that case, we first solve for the electron and ion temperatures without the contributions from the radiation-electron energy exchange. Each radiation group energy density is then solved for independently using the resulting electron temperature. Each group update can be written in the form of a linearized implicit backward Euler step and can be solved independently with iterative solvers like GMRES and Bi-CGSTAB using a BILU preconditioner. As long as the boundary conditions are such that the matrices are symmetric and positive definite, a preconditioned conjugate gradient method may also be used.

The update can be formulated in terms of the total energy for each group, which preserves the total energy to round-off errors. This scheme requires less computational time for preconditioning and for the Krylov solver than the coupled implicit algorithm. However it generally needs more message-passing in parallel computations. It is therefore not always guaranteed that the decoupled scheme is faster. The memory usage is always smaller.

Laser Energy Deposition Package for CRASH

We are developing a package to model laser energy transport and deposition in a self-consistent way within CRASH. This will allow us to simulate a complete radiative shock experiment in which all forms of energy present in the calculations are computed and evolved in time using a single, multi-physics model – the CRASH model. The addition of the laser package addresses one of the primary potential reasons for the morphology conundrum. Currently, CRASH simulations are being initialized from the results of HYADES-2D (H2D) that model the laser deposition and the concomitant transport and hydrodynamics for the first 1.1 ns. Although this is done with great care, differences in the code and model details make coupling CRASH to H2D one of the primary candidates for the morphological differences when compared to the experimentally observed shock structure. The other significant advantage is that it frees up valuable resources currently being used to run (H2D). Due to the lack of fidelity and robustness in the H2D rezoner, performing H2D simulations is very manpower intensive. Additionally, the time needed to obtain code revisions has proven to be problematic.

The laser energy transport and deposition model being installed in CRASH couples laser energy transport via a ray-tracing algorithm, based on the geometric optics approximation, with inverse Bremsstrahlung absorption calculated along the ray's path. The geometric optics approximation is appropriate if the electron density does not vary significantly over one wavelength.[15] The inverse Bremsstrahlung absorption mechanism is by far the dominant absorption mechanism under our laser conditions.[16]

An efficient parallel ray-tracing algorithm has previously been developed and implemented as part of the Space Weather Modeling Framework.[17] In the model each electromagnetic ray trajectory is treated as a curve with radius vector $\mathbf{r}$ in three-

dimensional space. The ray trajectory may be unambiguously determined if the distribution of the refractive index, $n(\mathbf{r},\omega)$, is know for the frequency and the initial position and direction of the ray is given. At each time step, the ray is traced by numerically solving

$$\frac{d\mathbf{r}^2}{ds^2} = \frac{d\mathbf{r}}{ds} \times \left(\frac{\nabla n}{n} \times \frac{d\mathbf{r}}{ds} \right)$$

for each ray where s is the arc length of the curve. The relative gradient of the refractive index, $\nabla n / n$, can be determined[17] from the plasma density distribution, $\rho(\mathbf{r})$ and the critical density, ρ_{cr}.

$$\frac{\nabla n}{n} = \frac{\nabla \varepsilon}{2\varepsilon} = -\frac{\nabla \rho}{2(\rho_{cr} - \rho)}.$$

The critical density is the density at which the refractive index goes to zero, in Gaussian units it is given by

$$\rho_{cr} = \frac{A m_p m_e \omega^2}{4\pi Z e^2},$$

where A, m_p, m_e and e are the mean atomic weight, proton mass, electron mass and electron charge, and ω is the laser frequency in vacuum. The algorithm is numerically solved using the Boris' scheme which automatically conserves the ray direction vector, $\mathbf{v}(s) = d\mathbf{r} / ds$.

Electron-ion collisions cause laser energy to be deposited into the plasma. The laser absorption coefficient α can be calculated from the effective electron-ion collision frequency, ν_{eff}, the plasma mass density and the critical density, as

$$\alpha = \frac{\nu_{eff}}{c} \cdot \frac{\rho}{\rho_{cr} \sqrt{1 - \frac{\rho}{\rho_{cr}}}}.$$

The effective electron-ion collision frequency is[18]

$$\nu_{eff} = \frac{2\pi}{3} \sqrt{\frac{8 k_b T_e}{\pi m_e}} \cdot \left(\frac{e^2}{k_b T_e} \right)^2 \cdot \left\langle N_i Z^2 \right\rangle \cdot \log \Lambda.$$

Here N_i is the ion density and $\log \Lambda$ is the Coulomb logarithm. The electric field will then propagate through the plasma as

$$E(\mathbf{r},t) \propto e^{i(\mathbf{k}_r \cdot \mathbf{r} - \omega t)} e^{-\mathbf{k}_i \cdot \mathbf{r}},$$

where the complex wave vector $\mathbf{k} = \mathbf{k}_r + i\mathbf{k}_i$ and $\alpha = 2Im(\mathbf{k})$.

To deposit the laser energy we first consider the energy emitted by the laser at each time step. The energy is distributed over the rays in accordance with the beam cross-sectional area and the local intensity distribution within the focal spot. While propagating along the ray, the energy is absorbed due to the inverse Bremsstrahlung process. The absorption over the arc length interval, ds, is the local energy deposition, E_{ijk}. The energy deposition is peaked near the critical density, $9 \times 10^{21} \text{cm}^{-3}$ for 0.35 μm-wavelength light, and it is sparse for the chosen algorithm of ray tracing with a finite number of discrete rays. Therefore, at each time step while advancing the equations of motion for the laser-produced plasma, the deposited laser energy is added to the right-hand-side of the electron heat conduction equation to be solved implicitly, as the source term

$$\frac{\partial E}{\partial t} = \nabla \cdot \mathbf{F} + \sum_{ijk} E_{ijk} \delta(\vec{x} - \vec{x}_{ijk}),$$

in which **F** is the electron heat flux discussed above. The delta-function is implemented by distributing the energy between the nearest cells with the total of the interpolation coefficients equal to one.

The implementation of the laser energy deposition package is currently being tested. The early results have been very promising with the ray integration taking less than 0.1% of the total simulation time. The results of one test that demonstrate a ray being strongly refracted near the critical surface are shown in Figure 12.

We are in the process of implementing verification tests for the laser package before moving on to applying the laser package to the full CRASH simulations; we expect to move on to that phase in a matter of weeks.

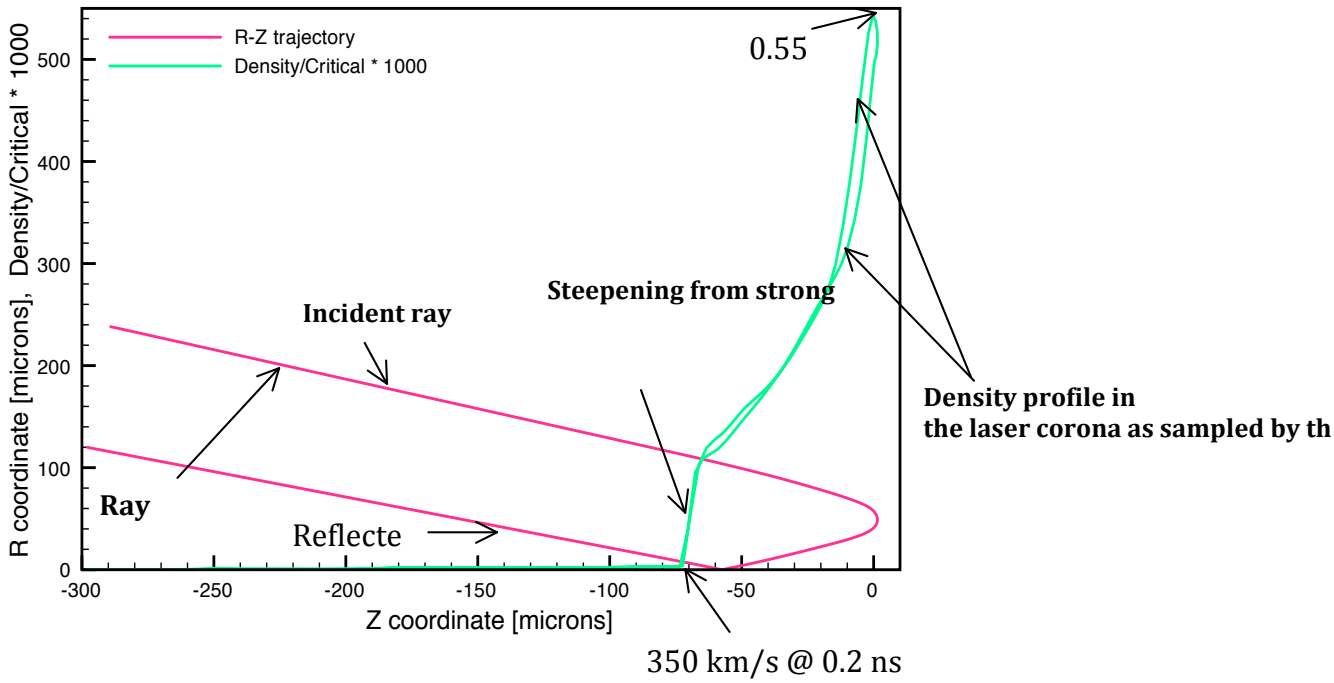

Figure 12. The red curve is the R-Z trajectory of a representative ray in a beam of rays at 0.2 ns of a 1.1 ns laser pulse. The ray starts a Z = -290 μm and propagates down and to the right. It is then refracted further down and intersects the symmetry axis at 60 μm.

Parallel Deterministic Transport (PDT)

Our highest-fidelity models may involve running the TAMU PDT code coupled to BATSRUS. Integrating the two codes has been put on hold, however, pursuant to a DOE ruling that such a combined code would at present be considered UCNI. We have made substantial progress on improvements to the PDT code, described below, have defined a first draft of the interface required to couple PDT to BATSRUS, and have done some testing of some elements of the interface. Our present focus is on improving the performance of PDT and on using PDT and CRASH to quantify the errors associated with the use of a diffusion model in CRASH.

Performance: efficient use of machines

Since our previous progress report we have made a concerted effort to improve the single-core performance and the parallel scaling of the PDT code for CRASH-relevant radiative-transfer problems. Our efforts have been fruitful. Our single-core performance has been improved by approximately a factor of 40, with our "grind time" (time to calculate one space-angle-energy unknown during a transport sweep) dropping from circa 15 ms to circa 350 ns. Our parallel scaling is such that on 4096 cores on the Hera machine at LLNL, our efficiency is 95% for a problem with 2048 cells per core, 10

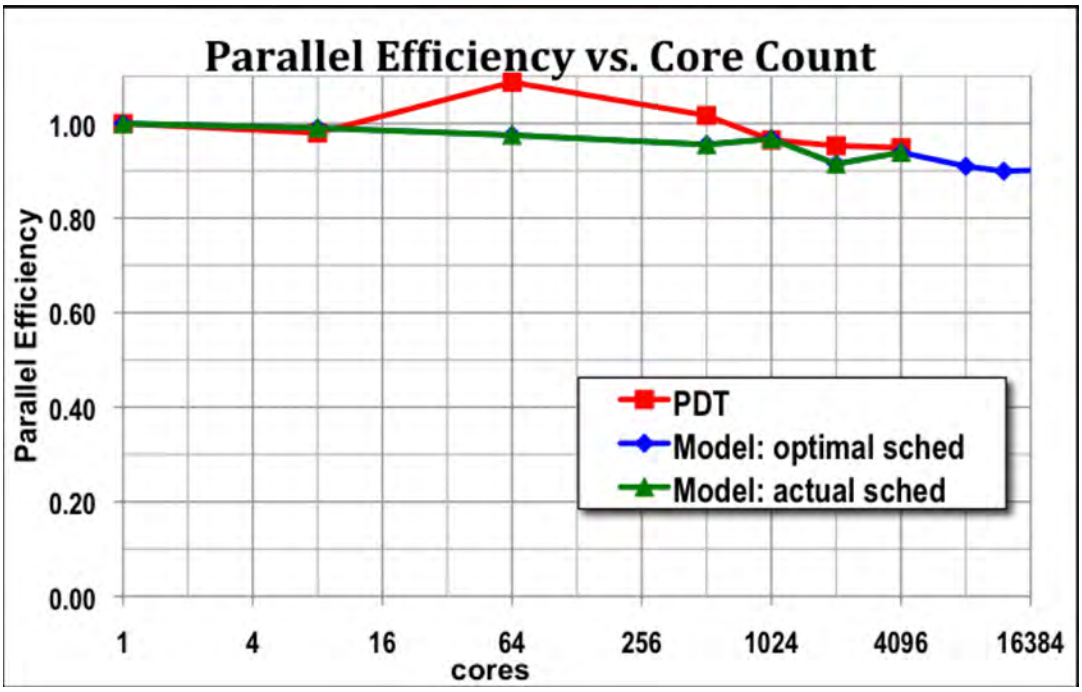

Figure 13. PDT Scaling on Hera, January 2011, 2048 cells per core. Efficiencies are normalized to the 1-core case.

energy groups, and the S8 level-symmetric quadrature set (which has 10 directions per octant). Our current and planned efforts in the performance realm are aimed at extending these excellent results to tens and hundreds of thousands of processes. At the time of this writing we have successfully run PDT on 32,768 cores on the ubgl machine at LLNL. As expected, our initial runs at this scale uncovered inefficiencies (mostly in unnecessary memory allocations) that we are now working to eliminate. Nevertheless, even with only 128 cells per core, our weak scaling study showed a decrease in parallel efficiency of only a factor of two when going from 8 cores to 32,768.

An important component of our work on parallel scaling has been the development of a theoretical model of parallel efficiency for various algorithms for cell-based "true" transport sweeps. A "true" transport sweep respects all upstream dependencies from boundary to boundary rather than using "old" angular intensities on internal interfaces. These dependencies could significantly reduce the parallel efficiency that is achievable with sweeps. A given sweep algorithm can be divided into three parts: 1) the partitioning of the problem domain among processes, 2) the aggregation of cells, directions, and energy groups into tasks, and 3) the scheduling algorithm that prioritizes tasks when multiple tasks are available for a given process at a given time. To date we have restricted ourselves to partitions that divide the spatial domain among processes, such that if a process owns a given cell it performs the calculations for all directions and energy groups for that cell.

We have focused on developing a provably optimal scheduling algorithm that will apply to any given partitioning and aggregation, and we have recently shown (early 2011) that

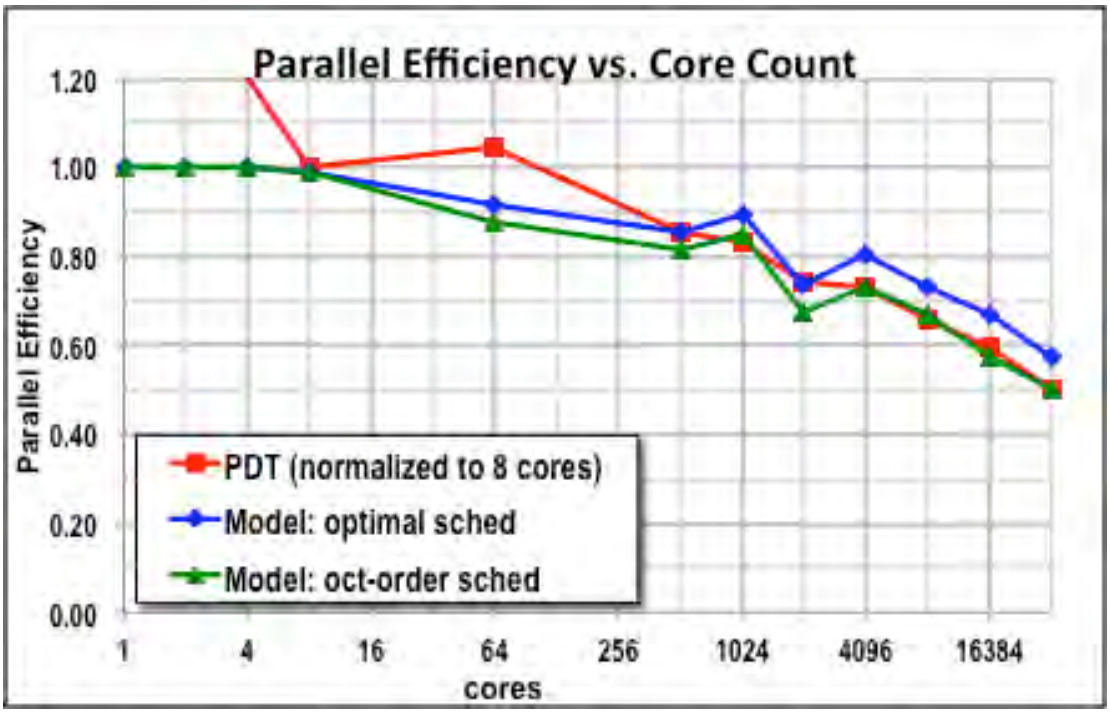

Figure 14. PDT Scaling on Blue Gene / L, late November 2010, 128 cells per core. Efficiencies are normalized to the 8-core case.

there are several slightly different algorithms that all produce optimal results for standard partitionings and aggregations. We have implemented one such algorithm in PDT and verified that it produces optimal results in that the number of calculational stages that it employs to complete a sweep is exactly the provably optimal number that it should employ.

The existence of such an optimal scheduling algorithm in PDT opens the door to even more significant optimization: optimization of partitioning and scheduling. That is, we are now working to develop optimization logic that will choose, for a given physical problem at run time, the partitioning and aggregation whose optimal schedule produce the minimum execution time and thus the maximum parallel efficiency. This requires a performance model that predicts parallel efficiency for a given partitioning and aggregation. We have developed such a model and tested it with PDT on the HERA and BlueGene/L machines at LLNL. Figure 13 presents recent results from HERA, including model predictions for an optimal schedule, model predictions for the schedule that PDT used (which we see was optimal), and actual PDT results. At the time of the October CRASH Review, PDT parallel efficiency dropped well below model predictions as core counts increased above 2048, reaching 85% at 4096 cores. We have tracked down and eliminated two issues, with the result that on the same problem PDT now achieves 95% efficiency on 4096 cores, which is what the model estimates it should achieve. We cannot yet claim that the model is accurate or that the PDT implementation is perfect – note that the two curves do not track perfectly over the full range from 1 to 4096 cores. However, these results are extremely encouraging.

As we have investigated the differences between PDT performance and model predictions, our research has proceeded along two fronts that should provide insight: 1) We are exploring PDT performance on other machines to test whether the HERA performance is unique to that machine. 2) We are porting PDT from its current PTTL library to the new STAPL library to test whether performance issues may be caused by old non-scalable implementations in the PTTL run-time system.

On the first front, Figure 14 presents our very early scaling studies on the BG/L machine at LLNL, circa late November 2010. We are pleased that – once we were able to compile the code with BG/L's rather old compilers – PDT ran without difficulties all the way to 32,768 cores (the largest count we have attempted so far). We are also pleased to note that the code performance does not fall off relative to model predictions on BG/L, and in fact tracks the performance model quite well from 512 cores to 32,768 cores.
However, the BG/L results present a new mystery that we are now working to solve: PDT loses a factor of two in efficiency (i.e., its grind time doubles) when we go from one core to eight cores on BG/L. (To highlight what happens at larger core counts and not obscure it with this 1-to-8-core puzzle, the figure below normalizes parallel efficiency to the 8-core case.) We have decided to postpone a serious investigation of this and other scaling issues until we have ported PDT to the new STAPL library.

Difference between transport and diffusion

Performance improvements to date have enabled us to use PDT to generate high-fidelity results of CRASH-relevant radiation problems. We have devised a CRASH-like radiation test problem to facilitate our UQ sensitivity studies, to study numerical convergence, and to quantify the difference between transport and diffusion. A sketch of this test problem is given in Figure 15.

As an example of the fidelity that we can achieve in this *two-dimensional* test problem, we can run this problem with 50 energy groups, 360 directions, and very fine resolution in the plastic ablation layer (zoning < 0.005 microns), out to 10 ns, on 1024 cores on the Hera machine at LLNL, over the course of a weekend.

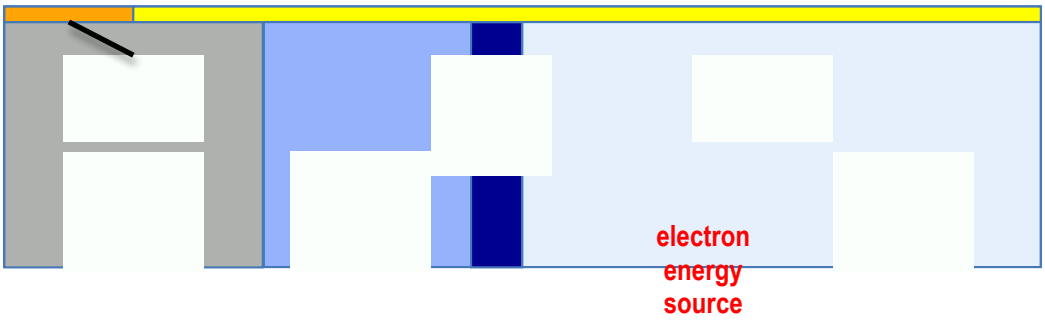

Figure 15. CRASH-like test problem. Radiation only; no hydrodynamic motion.

We are using this test problem to help quantitatively characterize the difference between diffusion and transport. An obvious approach for this is to compare CRASH multigroup diffusion against PDT multigroup transport with the same zoning and same multigroup opacities. Such comparisons are underway. We are focusing our attention initially on the ablation layer in the plastic, seeking to determine whether diffusion is causing a blow-off that is too rapid and/or too intense, thus possibly contributing to our overarching difficulty in simulating the morphology of the shocked xenon in our experiments.

It may be difficult to assign causes to differences that we will see between CRASH diffusion and PDT transport. The codes use very different time discretizations and different degrees of implicitness in various terms. The diffusion discretization in CRASH is also quite different (cell-centered finite-volume) than the transport discretization in PDT (discontinuous Galerkin). Thus, even if transport and diffusion should yield the same answer on a given problem it is not clear that PDT and CRASH will obtain the same answer except in the limit of very small spatial zones and very small time steps. To circumvent these difficulties we have developed a novel approach to quantifying the difference between transport and diffusion, and we are implementing this into PDT. The basic idea is that during a transport calculation, we can compute and edit the frequency-dependent source in each cell that would have to be added to discontinuous-Galerkin discretization of the diffusion equation in order for that diffusion discretization to produce the discontinuous-Galerkin transport solution. The size of this required source term relative to other terms in the equation is an indication of the difference between transport and diffusion, resolved in space, time, and energy. It is interesting to note that this source term can also be viewed as a *residual*, equal to the difference between the right and left sides of the transport equation when the diffusion solution is inserted.

Iterative algorithms

It is no surprise that even with the performance improvements described above our multigroup discrete-ordinates treatment of radiation transport requires substantial computing resources. Efficient numerical algorithms are of primary importance, because they allow a greater number of calculations with a given fidelity. This is especially significant given the predictive-science focus of the Center, which requires substantial numbers of calculations as part of the UQ effort.

We have developed a diffusion-based preconditioner to accelerate the convergence of our PDT transport iterations. At the time of this writing it has been implemented into the code and is undergoing initial verification testing.

Year 4 Transport Plans

Our first priority for the coming year is to quantify the differences between multigroup diffusion and multigroup transport on CRASH-experiment problems. This is vital to the central mission of the center, because the error introduced by employing diffusion instead of transport is potentially a major source of uncertainty and must be quantified or bounded. Given our current prohibition on coupling PDT with CRASH, this will be a challenge. However, we are prepared to meet this challenge using the two strategies described above: 1) PDT-to-CRASH comparisons, and 2) our novel algorithm for quantifying a measure of the difference between diffusion and transport. We expect to use a variety of test problems for these exercises, beginning with the CRASH-like test problem depicted above but also including snapshot problems taken from coupled rad-hydro simulations of actual experiments.

If regulations permit, we will devote considerable effort to coupling PDT with CRASH. This will make it conceptually much easier to quantify differences between transport and diffusion, but it will also carry considerable challenges (in implementation, verification, and resource utilization).

We will continue our work toward optimal parallel scaling and toward efficient implementations of PDT on the massively parallel architectures to which we have access. We expect to publish a paper that defines for the first time a provably optimal algorithm for executing true transport sweeps in parallel on orthogonal grids in 2D and 3D.

We will complete the migration of PDT onto the new STAPL library and further improve the library in response to observations its performance with PDT on CRASH-relevant problems.

IV. Experiments

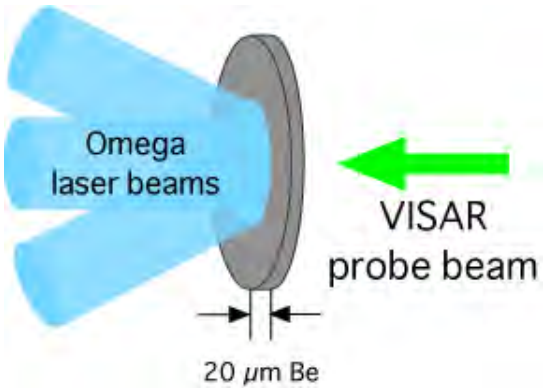

Figure 16. Target schematic showing a nominally 20 μ m Be disk irradiated with several laser beams. The VISARs and SOP view the rear surface of the target and measure shock breakout time.

During this period the CRASH team has executed experiments at the Omega laser facility on two days, with a third to follow in February 2011. We performed a "half-day" experiment in August 2010, obtaining the data at 20 and 26 ns needed for the UQ study discussed above. An example of these data was shown above in Figure 3. The most recent experiment, the Year 3 experiment, was in December of 2010, and continues in February. The Year 3 experiment aims to characterize the conditions of the radiative shock very soon after shock breakout, because we concluded that this period had a significant impact on predictive capability -- our analysis of the simulation output was that this time period has a very strong effect in the simulations on the long-term evolution of the structure. The results of our radiographic measurements have been published (or submitted) by CRASH graduate student Forrest Doss,[10-12] while results of the Year-2 experiments, described next, are in preparation for publication.

Year 2 experiments sought information to better characterize the laser-driven, initial state of the radiative shock experiment. These experiments consisted of a 2.5 cm Be disk with thickness ranging from 19 μm to 21 μm, measured to ± 0.5 μm. Out of 8 experiments there were 3 disks that were 19 μm thick, 4 disks that were 20 μm thick and one 21 μm thick disk. This yields an average disk thickness of 19.75 μm and a standard deviation of 0.7 μm. In each shot, a disk was irradiated with 10 Omega laser beams with a laser spot size of ~ 820 μm FWHM. The nominal laser energy of the 10 beams was 3.8 kJ. For this experiment the on-target laser energy averaged to 3.911 kJ ± 0.001 kJ. The range of laser energy for this specific set of experiments ranged from 3.837 kJ to 3.945 kJ with a standard deviation of 0.034 kJ. The laser pulse was a 1 ns square FWHM pulse with about 100 ps of rise and fall time. The nominal on-target laser irradiance was about ~7 x 10^{14} W/cm^2. The spatial profile of the irradiance is known.

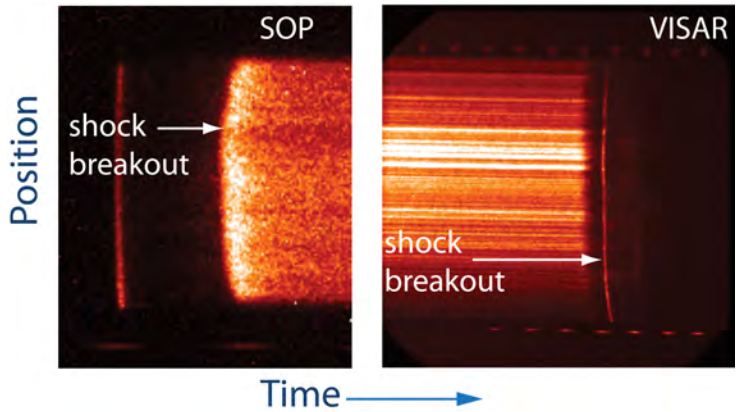

Figure 17. Typical SOP (left) and VISAR (right) data showing shock breakout.

The laser beams launch a shock into the Be disk and the amount of time it takes for the shock to move

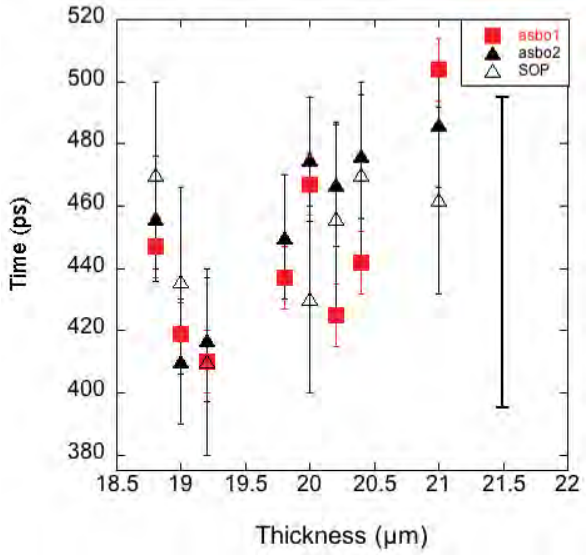

Figure 18. Shock breakout time for Be disks of 19, 20 and 21μm. Data points are offset in thickness in order to discern between individual experiments.

through the Be disk is measured. These measurements were made with three instruments for each experiment. Two of the instruments were each a Velocity Interferometer System for Any Reflector (VISAR), each set to a different sensitivity. A VISAR uses a laser of 532 nm wavelength to probe a surface and detect rate of change in the derivative of the optical path to a surface. This directly measures the velocity vs. time of the surface probed, from which one can infer average pressures. For the experiment reported here, the probe laser is reflected off of the rear (non laser-irradiated side) of the Be disk as shown in Figure 16. Since the Be disk is opaque to the probe laser light, only the shock exiting the rear surface of the disk is detected. This is referred to as shock breakout and the time when it occurs is referred to as the shock breakout time.

The third diagnostic used to measure the shock breakout time was a Streaked Optical Pyrometer (SOP). A SOP is a passive detector that records thermal emission on a streak camera which results in a 2D image showing the emission in space and time. SOP is also observing the rear surface of the target. As the hot shock emerges from the rear of the Be disk its emission will be recorded with the SOP yielding the shock breakout time.

Examples of the typical VISAR and SOP data from this experiment are shown in Figure 17. The SOP data is shown in the left panel where the bright emission indicates the shock breaking out from the disk. The VISAR data is shown in the right panel. In this case, the probe beam is reflected of the rear surface of the Be disk and a path length difference in the probe beams causes the bright fringes on the left. The shock breaking out of the disk is shown as the thin line to the right of the fringes. The observed curvature is real and is a consequence of the radial variation in ablation

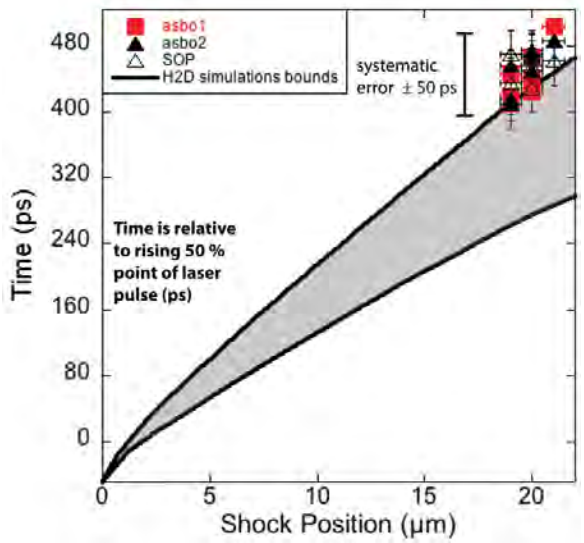

Figure 19. Results from 104 H2D simulations showing time vs. shock position compared to experimental data. The black lines indicate the range of results from the 104 H2D simulations.

Parameter	Input Range
Be γ	1.40 – 1.75
Flux limiter	0.05 – 0.075
Be thickness (μm)	18 – 22
Laser energy (kJ)	3.6 – 4.0
Wall opacity	0.7 – 1.4

Table 1. Input range of parameters varied in the 104 2D Hyades simulations.

pressure across the laser spot.

Both of these VISAR and SOP measurements can be calibrated in time using the timing fiducials seen at the bottom of both of the images shown in Figure 17. These fiducials are created with an optical laser that is timed to the laser used to irradiate the target to ± 50 ps. The resulting shock breakout measurements are shown in Figure 18. As mentioned previously 3 disk thicknesses (19, 20 and 21 μm) were used. However, in order to discern individual disks, the thickness of each disk has been offset 0.2 μm. The 3 data points for each disk are from the 2 VISARs and the SOP instruments. The vertical error bars on each point are due to the error in each diagnostic measurement and to the sensitivity of the measurement. The VISARs were the most sensitive and had errors of ± 10 ps and ± 20 ps while the SOP had a larger error of ± 30 ps. There exists a larger systematic error in the absolute timing due to the timing of the fiducial laser and the laser pulse used to irradiate the disk. This error of ± 50 ps is shown as a vertical bar on the right of the plot. The error in the disk thickness is ± 0.5 μm and is not shown on the plot. Note that on individual shots the shock breakout time recorded by each diagnostic agrees with the other diagnostics on that shot to within diagnostic error. Also, systematic timing error is the largest error and nearly encompasses the entire timing range observed. Under the experimental conditions described above the average shock breakout time was 450 ps.

A total of 104 H2D simulations were performed varying the Be polytropic γ, electron flux limiter, Be thickness, and the opacity of the polyimide wall. The majority of these parameters were chosen because a previous sensitivity study, performed with 1D Hyades, indicated that the shock position was most sensitive to these parameters. The exception is the wall opacity, which was studied because it could not be modeled in 1D simulations. The ranges of each parameter are shown in Table 1. The specific parameters used for each of the 104 Hyades simulations were determined using a space-filling, latin hypercube algorithm in order to efficiently sample the parameter space. A latin hypercube is a multi-dimensional sampling process, enabling a statistical analysis of the 5 parameters that are varied. Many studies use latin hypercubes in order to evenly sample a large parameter space without extraneous computing cost. The range of results of these simulations are shown in Figure 19, which also includes the experimental data. The experimental shock breakout time overlaps with some of the simulation results, but is later than many of the simulated values.

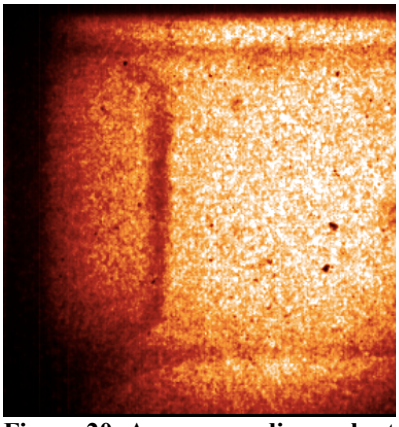

Figure 20. An x-ray radiograph at 3.5 ns after the laser pulse began. The shock has propagated about 380 μm from surface of the Be disk.

Year 3 experiments also focus on early time behavior; however, we sought to use x-ray radiography to diagnose the dense Xenon layer. Figure 20 is an x-ray radiograph imaged at 3.5 ns after the initial laser pulse irradiated the Be disk. The thin, dense Xe layer has moved about 380 μm. The thickness of the shocked Xe layer, projected along the diagnostic line of sight is about 50 μm thick, most of which is likely produced by a tilt of a few degrees with respect to the line of sight. Additional experiments in February 2011 will continue exploring early-time radiography as well as streak radiography of the Xe layer and the shock emerging from the Be disk.

V. CRASH Applications

We desire to see the CRASH code used for a variety of problems other than the primary CRASH experiments, for many reasons. Among these are the discovery of bugs, well-known to increase under such circumstance, the development of experiments that may be useful for uncertainty quantification, and validation exercises. We discussed the application of CRASH to designing radiative reverse shock experiments in the Summary Overview above, and discuss its application to hydrodynamic instabilities in the section on student research, below. Here we include some discussion of hydrodynamic experiment designs and x-ray driven simulations.

Non-radiative Variations on the CRASH Experiment

The proposed CRASH experiment for year 5 involves switching from a circular tube to an elliptical tube. Although the circular tube can be simulated in two-dimensional cylindrical geometry, modeling the elliptical tube requires three-dimensional simulations. One suggestion for a year 4 experiment was a non-radiative version of the proposed year 5 experiment. This requires generating a shock with a much lower velocity, which can be accomplished by using a thicker Be disk and reducing the laser energy. Since the Hyades code, which is used to generate the initial conditions for CRASH, is only two dimensional, the section of tube attached to the Be disk must have a circular cross section. Some type of nozzle or step is needed to connect the circular tube to the elliptical tube

Using the CRASH code to predict the results of the non-radiative experiment in advance could be used as a “dress rehearsal” for the year 5 experiments and would be an excellent test for the CRASH UQ process. The study has also been useful in pushing the limits of the code into regimes that have not often been used (large grids, large numbers of processors, large quantities of I/O, etc). This has led to a number of code improvements and has suggested the need for others.

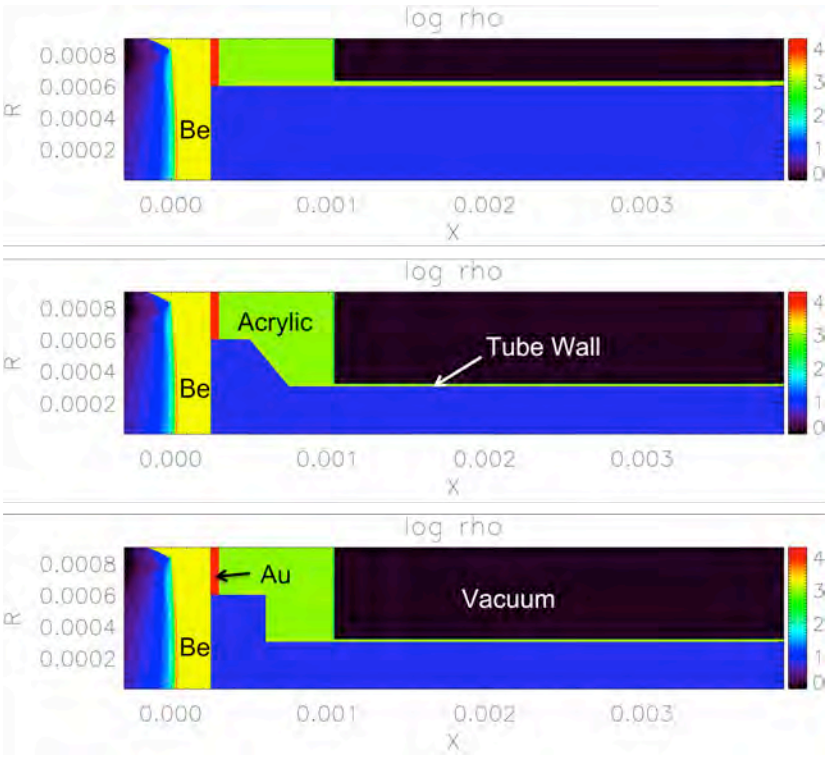

Figure 21. Initial conditions at 1.1 ns for the straight tube, nozzle, and step.

For the non-radiative case, the thickness of the Be disk was increased from 20 μm to 250 μm, and the laser energy was decreased from 3.8 kJ to 1.0 kJ. As a result, the shock speed decreased from ~200 km/s to ~20 km/s, well below the speed at which radiation becomes important. In addition, the diameter of the circular section of the tube was increased from 600 μm to 1200 μm. Three sets of simulations were performed. The first used a straight circular tube of diameter 1200 μm. For the other two, the circular tube was connected to the elliptical tube by either a nozzle or a sharp step. The axis ratio of the ellipse was 2:1. The three initial conditions at time 1.1 ns are shown in Figure 21.

Unlike the radiative case, at 1.1 ns the shock has not yet broken out of the Be disk. The results of the simulations for all three cases at time 200 ns are shown in Figures 22, 23, and 24, for a uniform grid of size 2400 x 480 x 480.

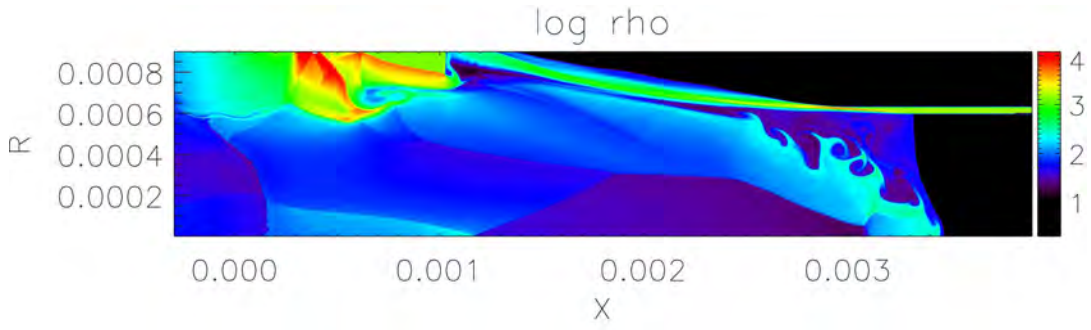

Figure 22. Circular tube.

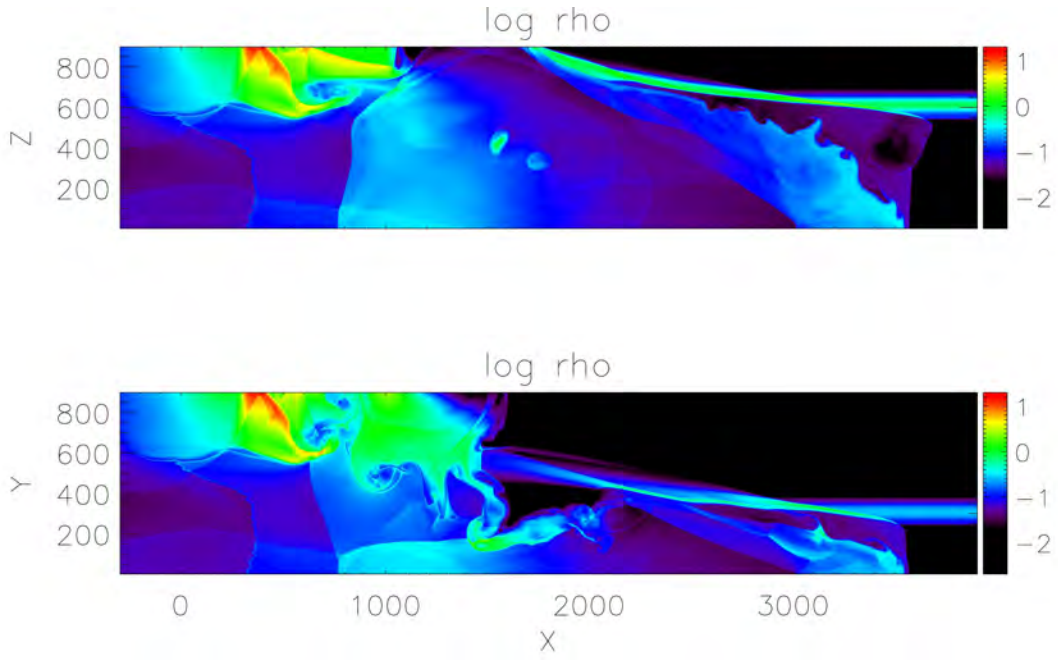

Figure 23. Elliptical tube with nozzle (top: y=0 plane, bottom: z=0 plane)

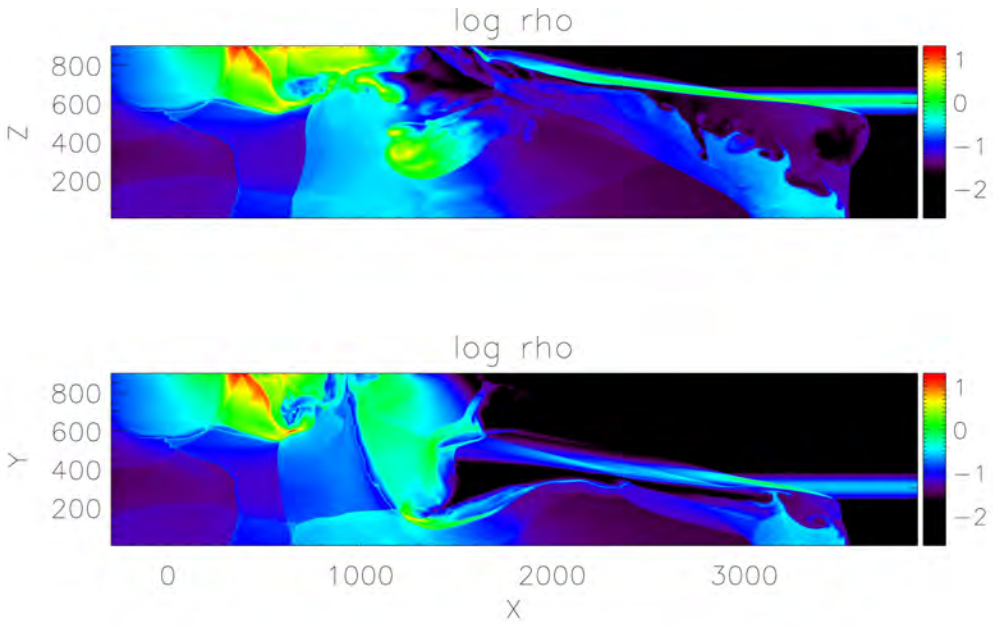

Figure 24. Elliptical tube with step (top: y=0 plane, bottom: z=0 plane)

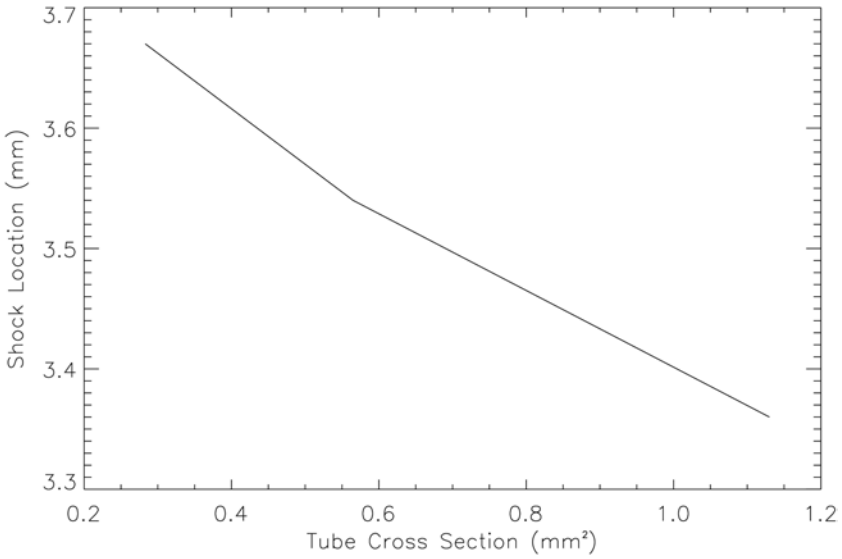

Figure 25. Variation in shock location resulting from changing the cross-sectional area of the tube.

Reducing the cross-sectional area of the tube increases the shock velocity slightly as shown in Figure 25. The results of this study do not show dramatic differences between the nozzle and step, which in practice will be determined by feasibility of target fabrication. In addition, we now have a set of parameters that provide an initial design of a three-dimensional hydrodynamic experiment, should we decide to pursue these.

X-ray driven initialization for studying shock structure

Among the current challenges facing the CRASH project is explaining the persistent discrepancy between shock structures seen experimentally and those obtained by the CRASH code using the "best" initial conditions and input physics. In particular, CRASH simulations show a much richer structure at the primary shock front than is inferred from experimental radiographs. Most simulations show significant sloping, curvature, or complex shock structure, while experiments suggest the shock is nearly planar, with some local structure or modulations.

To improve our knowledge of the origins of the structure in the CRASH simulations, the CRASH team has made several studies of x-ray-driven systems that generate simulated shock waves in a CRASH-like environment. In these studies, detailed laser physics (normally supplied by the Hyades code) has been replaced by radiative boundary conditions, which effectively subject matter near the relevant boundaries to irradiation by x-rays. This also enabled us to directly compare results of Hyades and CRASH for a CRASH-like x-ray-driven problem, with results shown above in the Summary Overview section. Here we consider the problems of ablation of low-Z walls and of producing an x-ray-driven analog of the CRASH problem.

Ablation of low-Z walls by x-ray ablation

One of the questions relating to the production of structure in the primary CRASH simulations is whether the generation of the wall shocks is being adequately resolved. We have developed a semi-analytic description of this problem, and have carried out simulations of it using CRASH and Hyades, with the aim of generating a publication about this problem. Here we discuss the CRASH results. We set up a one-dimensional problem analogous to what might be observed radially within a shock tube. We study the resulting ablation of wall material into the interior of the shock tube and the formation of a wall shock analogous to that seen in full CRASH simulations (Figures 26 and 27). We also observe additional shock and heat fronts that propagate radially outward within the wall itself. These tests employ a simplified equation of state, which assumes a monatomic ideal gas of fully ionized Be everywhere in the computational domain, and a simple analytic model for the opacities based on inverse Bremsstrahlung absorption:

$\kappa_{Planck} = 3.0 \times 10^{10} (\rho^2 / T^{7/2})\ cm^{-1}$]

and

$\kappa_{Rosseland} = 4.2 \times 10^{9} (\rho^2 / T^{7/2})\ cm^{-1}$]

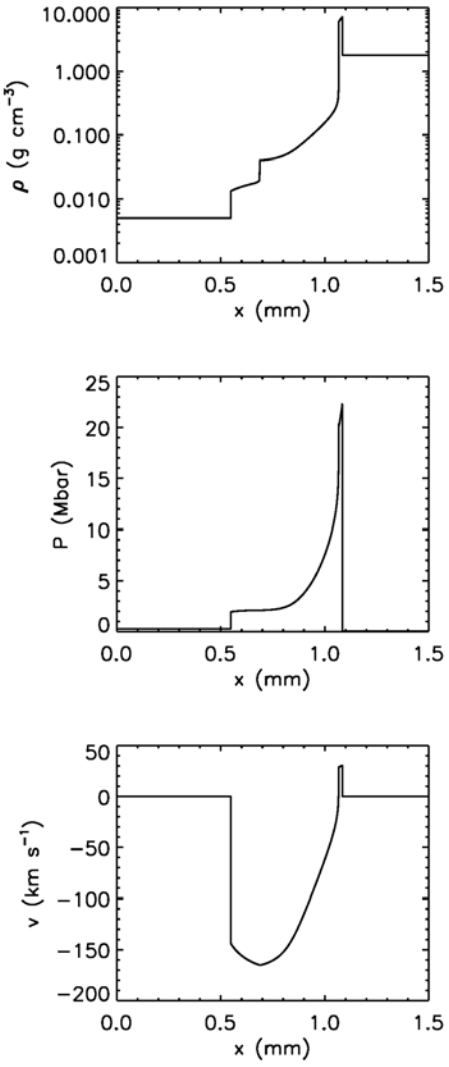

Figure 26. CRASH-code results for density, pressure, and velocity show good qualitative agreement with our semi-analytic analysis) The rightward moving dense shock and heat front are both present as is the leftward-moving forward shock. The latter corresponds to the wall shock of the full CRASH problem.

Even with these simplifying assumptions, the model has proved useful in its predictions of the extent of the wall shock and the degree of ablation from the polyimide wall of the full CRASH problem. The simulations show that the density of shocked gas behind the wall shock equals that of the rarefaction from the dense wall at the contact surface between the two materials. The results showed that our well-resolved CRASH simulations do adequately capture the wall-shock dynamics, but that simulation of the shock structure becomes much less adequate as resolution decreases. We expect to further explore wall ablation using more realistic treatments for the materials of interest.

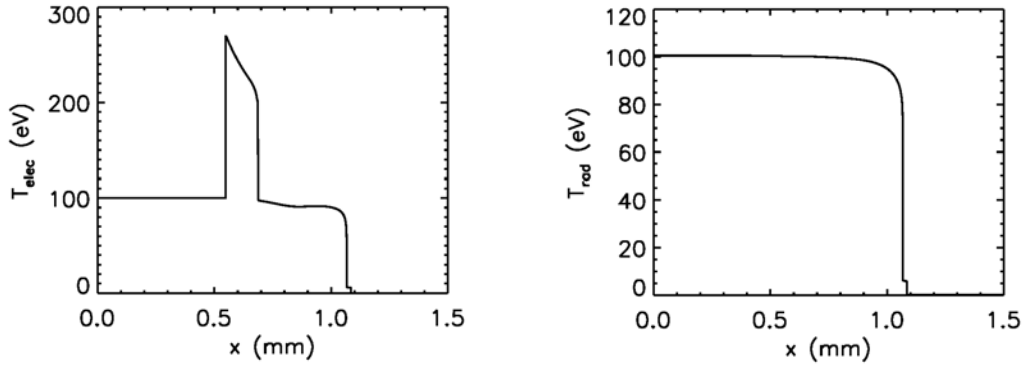

Figure 27. CRASH-code results for the same simulation as Figure 24, showing profiles against distance in mm of electron temperature in eV (left) and radiation temperature in eV (right). Of note is the region of isothermal rarefaction in the post-shock region to the right of the leftward-propagating wall shock, whose location is shown by the broad spike in electron temperature. Also of note are the limited penetration of the radiation into the denser wall material for $x > 1{,}0$ mm and the small step corresponding to the shock within the wall to the right of the expansion heat front where the radiative energy is deposited.

A CRASH-like problem initiated with x-radiation

We set up initial conditions like those of the CRASH problem. However, instead of initializing with Hyades output, we drive the problem from $t = 0$ with x-radiation at the left-hand boundary for a finite time. This implementation approximates the simulation of an experiment performed using a hohlraum rather than a direct-drive laser source. Initially implemented using gray transport and three materials, over the course of the past year, we have implemented the full CRASH physics, including multigroup flux-limited diffusion for the radiation, all five materials of the CRASH experiment, and electron heat conduction.

We find that based on choices for three adjustable parameters—the effective x-ray temperature at the boundary, the duration of the x-ray pulse, and the thickness of the Be disk—it is possible to produce nearly planar shocks that closely resemble experimental results (Figures 28 and 29). This strongly suggests that the anomalous structure seen in the full CRASH simulations is not the result of a feature inherent in the CRASH algorithm; neither is it likely the result of coding error. Instead, it seems that the evolution shock structure is a sensitive function of initial conditions used in the simulation. In support of this argument, we also find that, with this initialization model, if the energy imparted by the x-rays into the system is above some threshold, curvature of the shock fronts is established. The structure of these curved fronts closely resembles that seen in the full CRASH simulations using a Hyades initialization.

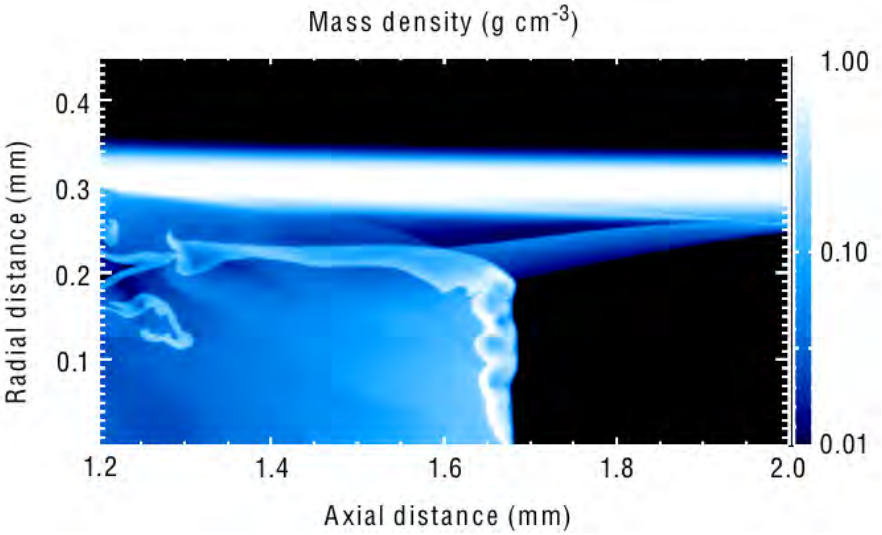

Figure 28. Close-up of a 170-eV x-ray-initiated simulation of the CRASH problem, showing the density structure near the shock front, including the wall shock and deflected shock. The image shown is at 12.0 ns after the x-ray source has been turned off (corresponding to a time of 13.0 ns in the analogous CRASH experiment). The simulation used CRASH v.2.1 with using complete Version 2 physics and was run with 16 radiation-energy groups with a range of 1.0 eV to 2.0 keV.

An interesting feature observed in both x-ray- and Hyades-initialized models is instabilities that develop along the interface between Be and polyimide as Xe becomes entrained behind the shock. Such instabilities are not presently seen in the experiments, but it is uncertain whether they could be detected with diagnostic methods used to date. In any event, Figure 30 demonstrates that, in numerical simulations, the degree of instability observed is a function of the resolution of the model. In contrast, the position of the shock remains independent of resolution. Figure 31 shows details of the post-shock density. Signs of both Kelvin-Helmholtz and Rayleigh-Taylor instabilities are present.

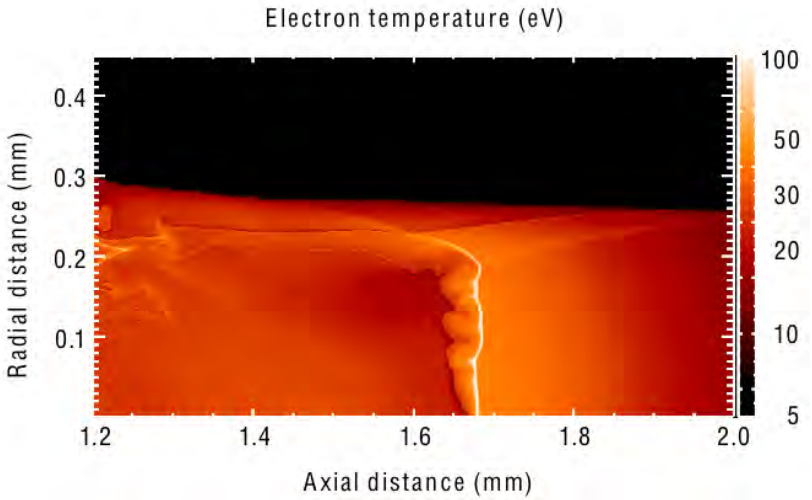

Figure 29. The same simulation shown in Figure C, but showing electron temperature

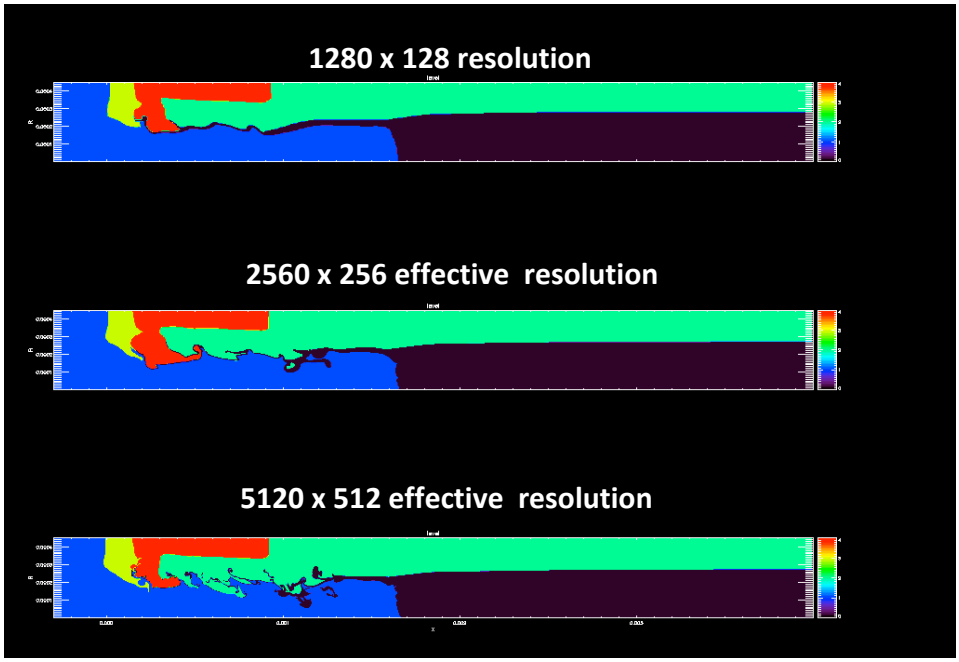

Figure 30. Level diagrams for three different simulation resolutions showing material interfaces for the near-optimally tuned run at 12.0 ns after the initial 170-eV x-ray source has been turned off. Although the positions of the forward Be–Xe interfaces are very similar, the character of the entrained Xe and the post-shock Be–Xe–Pl interfaces are very different. The more resolved case shows signs of shear flow leading to a possible Kelvin-Helmholtz instability. Further evolution also exhibits a possible Rayleigh-Taylor instability along the same interfaces.

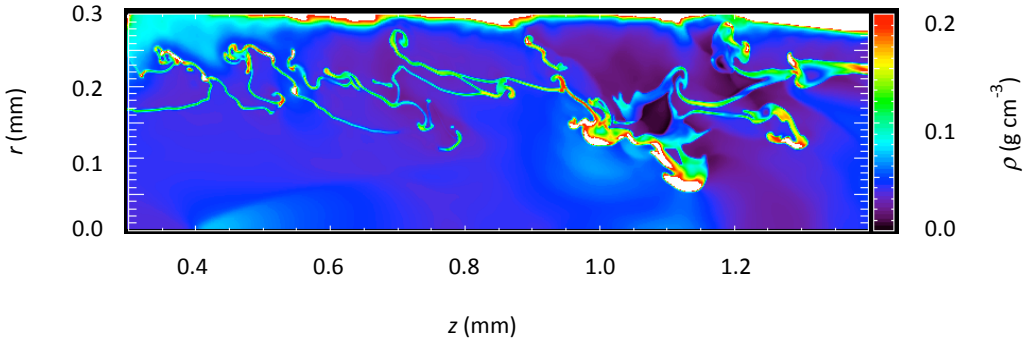

Figure 31. Density in a portion of the post-shock region 170-eV x-ray-initiated simulation of the CRASH problem. Like the previous Figures xx and xx, the image shown is at 12.0 ns after the x-ray source has been turned off (corresponding to a time of 13.0 ns in the analogous CRASH experiment). The complex pattern that results shows high-density entrained Xe sandwiched between lower-density Be (below) and ablated polyimide tube material (above). The structure suggests that the post-shock flow is subject to both Kelvin-Helmholtz and Rayleigh-Taylor instabilities.

V. Educational Status and Plans

Our current roster of graduate students associated with the CRASH center come from seven departments at Michigan (Aerospace Engineering; Atmospheric, Oceanic and Space Sciences; Applied Physics, Mechanical Engineering, Nuclear Engineering and Radiological Sciences; Mathematics; Statistics) and two departments at TAMU (Computer Science, Nuclear Engineering). Students are funded directly by the grant, by fellowships from cost sharing, and by other fellowships or grants but doing research supported at least in part by CRASH. A total of 13 students have spent one or more summers at an NNSA lab. A statistically higher-than-expected seven students visited the labs in 2010; we are working on setting up 2011 visits for two students (see Table), and have good contacts in both cases.

Table. Students seeking to spend time at an NNSA lab in 2010.

Student	Lab	Contact
Nick Patterson	Pending	Pending
Andrew Till	Pending	pending

Students, besides meeting with their individual advisors, attend meetings of the group roughly every two weeks. These meetings consist of a mix of review talks, introducing members of the group to the underlying technologies of the CRASH center, and specific students speaking about their research. In addition, students were involved in 24 of the posters presented at the annual review.

This year saw the completion of our first course offerings related to predictive science. In fall 2009, a new course was offered at TAMU. Its emphasis was on verification, validation, sensitivity analysis and uncertainty quantification. Prof. Ryan McClarren was the lead instructor; he developed and offered the course, with 10 students from a number of departments in attendance. In the winter semester of 2010, a new course was taught at Michigan by Profs. James Holloway, Vijay Nair and Ken Powell. It focused on input/output modeling, screening and sensitivity analysis and uncertainty quantification. Students developed a simple simulation code, and exercised some basic uncertainty quantification and sensitivity analysis on that code. In the latter half of the semester, students were organized into groups of three or four, to apply the techniques they have learned in the course to simulation codes they are using in their research. The course met three times a week: two lectures and one computer-lab session. Twenty students attended the course. Several of these students, and several from outside the CRASH project, are enrolled in the Scientific Computing certificate program. This program requires several courses in numerical methods, several courses in computer science, in addition to the requirements for the PhD in the student's home department. Some of the CRASH students enrolled in the certificate program are pursuing the Predictive Science track of the Scientific Computing certificate.

VI. Graduate Student Research

Computational and Statistical Students:

Anthony Barbu (Advisor: Adams) has continued his work on diffusion preconditioners for radiation transport calculations. His formulation builds a diffusion preconditioner for an arbitrary discontinuous finite-element-method (DFEM) transport discretion by manipulating the cell-wise matrices that the DFEM uses in its transport solution. He has coded his formulation in PDT in such a way that the diffusion coding does not know the details of the particular DFEM, but simply works in terms of the DFEM's cell-wise matrices. This means PDT now has a preconditioner that is "consistent," in a certain important way, with whatever DFEM is used for the transport. When a new DFEM is added for transport, the preconditioner coding does not need to be altered. At present the implementation uses a gray diffusion preconditioner for the iteration on absorption rate density, which is nested inside an iteration on temperatures. In the near future we will explore potentially more efficient strategies that place the temperature iteration inside the transport iteration on absorption rate density.

Jason Chou (Advisors: Fryxell and Drake) has been applying the CRASH code to calculations of Rayleigh-Taylor Instabilities (RTI) These provide a good way to compare the various hydrodynamic solvers in CRASH. Even though pure hydrodynamic RTI is well understood, this investigation is necessary for us to understand the behavior of CRASH for more complicated problems, such as MHD RTI. Jason has found that there are conditions in which the Linde numerical scheme converges to the expected exponential growth rate, as Figure 32 shows. This particular solver is comparatively diffusive. When the instability is initiated by small-amplitude perturbations of the shape of the interface, the code requires 24 zones per wavelength for growth and 128 zones to get the timing to within 10%. Growth is achieved more easily with this solver when a velocity perturbation of larger equivalent amplitude is used. Using the Godunov option in the code produces growth with much fewer zones per wavelength. We continue to accumulate knowledge about the behavior of different numerical schemes with combinations of various parameters on this problem.

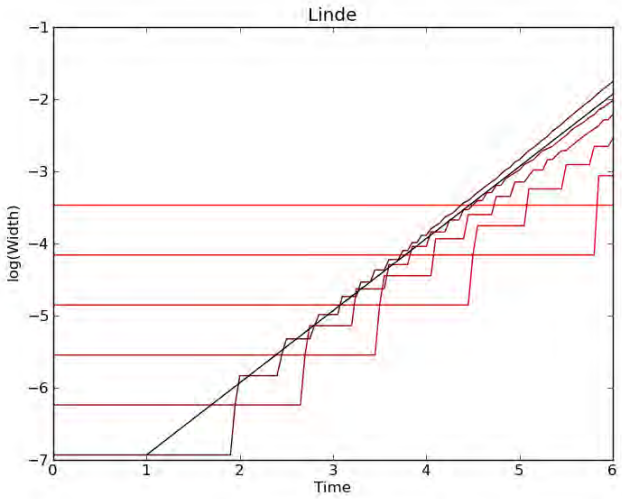

Figure 32. Amplitude vs time for resolutions increasing by factors of 2 from 32 zones per wavelength to 1024 zones per wavelength, using the Linde solver with certain settings for a pure RTI problem. The expected growth rate is shown as a solid black curve.

Jarrod D. Edwards (Advisor: Morel) completed this year a study related to the development and testing of several variants of the Trapezoidal/BDF2 time discretization scheme with application to nonlinear radiative diffusion. He also submitted a paper to the Journal of Computational Physics, which has been published in the February edition: Jarrod D. Edwards, Jim E. Morel, Dana A. Knoll, "Nonlinear Variants of the TR/BDF2 Method for Thermal Radiative Diffusion," Journal of Computational Physics, Vol.230, 1198-1214 (2011). During the next year he will be developing a second-order accurate rad-hydro scheme coupling the MUSCL-Hancock hydro method with the TR/BDF2 time discretization and the linear-discontinuous Galerkin spatial discretization for the grey radiation diffusion equation.

Adam Hetzler (Advisor: Adams) has returned to his work on dimension reduction and uncertainty quantification applied to opacities. He is currently exploring the sensitivity to small changes in ionization potentials and energy levels of the opacities that are calculated by the CRASH opacity software. Recent results for Beryllium show a strong sensitivity to small changes in certain ionization potentials, in some temperature ranges and given certain values for other ionization potentials. That this happens only in certain temperature ranges and for certain values of other uncertain parameters is an indication that linear sensitivity analysis is not applicable to this problem. By strong sensitivity we mean, for example, that Planck mean opacity can change by more than 50% in response to a change of less than 1% in one ionization potential, with all other parameters fixed. We will continue to explore and characterize these sensitivities, with the goal of quantifying uncertainties in CRASH-relevant quantities of interest as functions of the uncertainties in fundamental inputs such as ionization potentials.

Tiberius Moran-Lopez (Advisor: Holloway) A Reynolds-averaged Navier–Stokes mean flow equations turbulent system is being developed to model the effects of turbulence coupled to an equilibrium diffusion radiation model, where radiation and matter are in thermal equilibrium. Gradient-diffusion and similarity closure approximations are generalized to account for radiative effects. The mean radiative flux introduces additional unclosed terms from the Reynolds averaging that are addressed by proposing new closures and developing transport equations for temperature and density variances. A code to model this case is under development. A simplified model study can be conducted by assuming that the radiation energy density and opacity are uncorrelated in the Reynolds-averaging process; a code to model this case has also been developed, but the current explicit code needs to be made semi-implicit to allow progress. Rankine–Hugoniot analyses for the turbulent equilibrium diffusion model have also been performed and post–shock velocity and total pressure relations obtained, which lead to classical results when radiation and turbulence are neglected. Development of this model is intended to contribute to an improved understanding of high–energy–density and astrophysical phenomena in which both radiative and turbulent transport are important.

Over the past year**, Colin Miranda** (Advisors: Fidkowski and Powell) has applied gradient-enhanced response surface methods for uncertainty quantification (UQ) to a radiation-hydrodynamics test case, using a discontinuous Galerkin solver with adjoint capability. This task involved prior testing using an analytical input-to-output model,

which was debugged early this year. The radiation-hydrodynamics application required modifications to an existing in-house CFD code written in C and script-based coupling to Matlab pre- and post-processing. Based on the success of this work, a planned review paper on gradient-enhanced response surface methods turned into an application paper focusing on adjoint-based UQ for solutions to the radiation-hydrodynamics equations. The journal paper is in the final stages of preparation and will be submitted in the middle of this semester.

Pooya Movahed (Advisor: Johnsen) has has extended his parallel low-resolution (MUSCL) and high-resolution (WENO) codes to three dimensions and has started to study the hydrodynamics of shock-accelerated turbulence and multi-material mixing. After verification and validation of the code, he has carried out simulations of the Richtmyer-Meshkov instability in various configurations, including re-shock, multiple fluid layers and strong shocks (with Mach numbers up to 20). His results show that the MUSCL framework performed surprisingly well compared to the high-order accurate scheme for the initial instability growth. Based on these results, novel hybrid shock-capturing and low-dissipation approaches are being developed. From a physics viewpoint, Pooya is investigating the late-time behavior of the flow field and characterizing the turbulence. Short-term future work includes accurate implementation of physical diffusion. In the long term, transition to turbulence and the mixing transition will be studied, and the limits of low-dissipation methods will be pushed in problems with strong shocks, e.g., the non-radiative CRASH problem.

Tara Pandya (Advisor: Adams) has continued her work on long-characteristic (LC) methods for spatial discretization of radiative-transfer problems. LC methods now dominate deterministic transport calculations in nuclear reactors, largely because of their accuracy and their ability to treat complicated geometries. LC methods also offer potential for significantly improved parallel efficiency relative to methods that solve an entire spatial cell at a time. These accuracy and parallel considerations motivate us to explore the extension of LC methods to radiative transfer. The first essential extension is in the spatial shape that is assumed for the collisional source in each cell. In reactor analysis constant or linear source distributions work well, but these will fail miserably in radiative transfer given cells that are optically thick and diffusive. We have chosen to employ the same PieceWise Linear (PWL) basis functions that have been used successfully in DFEM transport. Tara has implemented and tested her LC scheme in two dimensions and is now working to implement it in 3D. We expect to compare LC and DFEM solutions on the CRASH-like test problem in the near future. We also expect to develop parallel sweeping algorithms that will be more efficient than today's cell-based algorithms.

Nick Patterson (Advisors: Thornton and Drake) has performed research on numerical treatment of mixed cells. These cells contain multiple materials, which are indicated for example by level set functions. He examined various methods of computing the effective diffusivity for mixed cells, and compared their convergence to accurate solution as the resolution is increased. Currently, his efforts are devoted to applying the Support Operator Method (SOM) to improve the discretization of the diffusion equation with

tensorial anisotropic diffusion coefficient. This method conserves flux between each cell, preserves the gradient and divergence operations inherent in the continuous case, and leads to a symmetric positive definite matrix equation, which allows the use of more accurate iterative solvers. Using this approach, we aim to develop an algorithm that increases the accuracy of simulations that involve mixed cells without significantly increasing computational time and memory requirements. Successful development and uncertainty quantification of such approach would benefit the CRASH program as a supporting code, which could ultimately be incorporated into the CRASH code. Nick Patterson recently succeeded in formulating the matrix elements for this case. His work has benefitted from the input from a CRASH team member, Jim Morel from Texas A&M as well as assistance from Scott Runnels, a Los Alamos National Laboratory scientist, who has an extensive experience with the SOM. We are bringing in Dr. Runnels for a CRASH seminar to further develop this collaboration.

Patrick Poon (Advisor: Stout) is working on robust methods for identifying features in the observed and synthetic radiographs. They are based on the fact that images contain several gross features, such as the shock front and beryllium, that are differentiated by their optical density. Using vertically integrated intensity, the software uses dynamic programming to find optimal subdivisions into a specified number of regions. These can be refined by horizontally integrated intensity. The techniques are robust in that they only assume that certain features are there in a known order, but make no assumptions about, say, their thickness or optical density.

Tim Smith (Advisor: Rauchwerger) has continued his work on the STAPL library in general and on the pRange component in particular. He is also part of the team that is currently porting PDT from the pre-STAPL library (PTTL) to the new STAPL library. We have always known that the new STAPL library, which is designed for high process counts, is an essential part of PDT's path to efficient use of massively parallel architectures. Tim is participating in scaling studies and other performance tests and is using the results to evaluate differences and similarities between the STAPL and PTTL versions of PDT. This work will continue as we proceed toward our goal of efficient CRASH calculations on machines with very high process counts (tens to hundreds of thousands of processes).

Dave Starinshak (Advisor: Karni) has been working on a simplified version of the CRASH model, that is simple enough to use for algorithm development purposes, while still retaining the essential physics of the more complete model, and with it its computational challenges. In its CRASH-like version, numerical solutions for this model exhibit noise and other inaccuracies near material interfaces that lead to poor quality of results. Dave developed a two-material upwind solver that addressed and pretty much cured the problem of oscillations, implemented and tested it extensively. While going over the derivation of the simplified model itself, Dave concluded that there was a better way to incorporate one of the simplifying assumptions. This lead to a different simplified model which was similar but not identical to the one we were handed. He redeveloped upwind multimaterial numerical techniques for this new model, implemented and tested them extensively. And, after learning more about the CRASH solver, he has developed

a two-material oscillation-free HLL solver that appears to be only a small but important modification of the method that is being used in CRASH. He has already extended his method to two space dimensions and is now in a very good position to address numerous issues including sensitivity of Xenon mass conservation to details of level-set approximation, and level-set strategies for three-material flows. We hope his study will shed light on interfacial instabilities, material entrainment and other morphological puzzlements observed in the CRASH code.

Hayes Stripling (Advisor: Adams) recently completed his M.S. thesis and a journal paper (accepted) on our "Method of Manufactured Universes," which is a methodology to assess the performance of various UQ approaches and their embodiments in software. He has also participated in the application of Bayesian MARS techniques to CRASH UQ problems. He will spend summer 2011 learning new methods and ideas as part of a group at ANL that specializes in UQ, and he will bring this new knowledge to the CRASH project. One focus of his summer studies will probably be uncertainties that arise from error propagation in a nonlinear transport problem in which the material-interaction coefficients depend on the history of the particle intensity. The application behind this is nuclide production and depletion in nuclear reactors, but the lessons learned may apply to propagation of errors in radiative transfer, in which the opacities depend on temperature, which depends on the history of the radiation intensity.

Over the past two and a half years under CRASH support, **Daniel W. Zaide** has been researching numerical shockwave anomalies in hydrodynamics under Professors Ken Powell and Phil Roe. This work examines anomalies associated with the simulation of strong shockwaves in a shock-capturing framework, such as in simulations done by the CRASH center. Particularly problematic is that of wall heating, best illustrated by the Noh problem. This anomaly manifests itself as a severe nonphysical temperature overshoot in a stagnation region, such as those in near wall regions and can lead to premature wall ablation and chemical reactions in numerical simulations. Also examined are the carbuncle phenomenon and slowly moving shockwave problem, two other numerical shockwave anomalies. By examining all of these in the same context, Daniel hopes link these phenomena and to understand the driving mechanisms behind them, potentially leading to a general purpose cure for these pervasive errors. With CRASH support, Daniel has been able to present his work at several conferences such as APS Fluids and the International Conference of CFD and currently has several conference publications in preparation in the upcoming year. Daniel was also able to spend the 2010 summer as a research assistant at Los Alamos National Laboratory, under the supervision of Dr. Robert Lowrie. In the future, Daniel intends to extend his work from hydrodynamics to radiation hydrodynamics to better impact the CRASH project.

Zach Zhang (Advisor: Nair) has worked on comparison of methods for modeling and predicting the outputs in large-scale computational models. The Gaussian Stochastic Process (GSP) has become the preferred approach for modeling and predicting the outputs of large-scale computational models. It is usually used in a Bayesian framework so that the predictive distribution of the output can be computed using Markov Chain Monte Carlo methods. One of the appealing features is that it results in an interpolation of

the output at the observed experimental settings, if the output is observed without error. One part of Zach Zhang's PhD dissertation compares the predictive performance of the GSP method against modern nonparametric regression approaches: multivariate regressions splines (MARS), mulitvariate regression trees (MART), and smoothing splines (SS). We have compared the methods on a broad array of test cases, ranging from smooth additive functions with no interactions to complex functions with interactions. The results shows that MARS and SS outperform the GSP approach in general. This is especially so when there are several input variables which are unrelated to the output variable. The regression-based approaches are easier to interpret and for screening the important input variables. The computational advantages of the various approaches are currently being studied. We expect two papers based on this work to be submitted within the next 3-4 months.

Experimental Students

The research of the experimental graduate students has been supported at least in part by CRASH, but also by the Stewardship Sciences Academic Alliances program and the National Laser User Facility program, both funded by Defense Sciences within NNSA, and by DTRA. The advisors of these students are Paul Drake and Carolyn Kuranz, in various combinations.

Graduate student **Forrest Doss** in continuing work begun by Dr. Amy Reighard Cooper, now employed by LLNL and doing shots on NIF. Amy developed the radiative shock experimental platform that is the basis for much of our further work with radiative shocks. This platform uses Omega to irradiate a Be disk for 1 ns at ~ 7 x 10^{14} W/cm^2, accelerating the Be to above 100 km/s and launching a shock into a gas-filled shock tube at an initial velocity near 200 km/s. Using Xe or Ar gas creates a radiative shock, in which radiation from the shocked material heats the upstream layer. The energy loss from the shocked layer in turn leads to a large increase in its density. In the Xe case, the shocked layer becomes optically quite thick to the thermal radiation (at near 50 eV). Amy published a number of papers describing her work to develop this system and initial observations of it.[19-22] Some additional papers related mainly to the theory of such systems were published by Prof. Drake and collaborators.[7,23-25]

Forrest Doss was subsequently challenged to understand the many interesting details that can be seen in the radiographs of the radiative shocks in Xe. These are illustrated in Figures 1 and 3 above. Forrest has made great progress in this. He was the person who identified the features labeled in Figure 1 as wall shocks, produced when radiation from the primary shock ablates the walls of the shock tube. He did this first by examining Amy's radiographs in the context of simulations he was doing using HYDRA. He then obtained improved data like that shown in the figures, in which the wall shocks are very evident, and published the results.[9] He also has published an analysis of the reproducibility of the properties that may be observed in the radiographs.[10] In the radiographs, one can see structure in the dense Xe layer that is probably related to a variant of the Vishniac instability, well known to cause modulations in thin, expanding

astrophysical shells. Forrest has submitted a paper[26] on the theory of the modified instability to the Astrophysical Journal, and is continuing experiments to attempt to find clearer evidence of it. He also has a paper in submission describing more completely the flow both ahead of and behind the primary shock,[12] based on the invited talk he gave at the Division of Plasma Physics of the American Physical Society meeting in November, 2010.

Graduate student **Tony Visco** was challenged to better diagnose the axial structure, using the Ar-gas variant of this type of system (where features are spread out enough that one can hope to diagnose them. He has done experiments at Omega that used UV Thomson scattering, streaked optical pyrometry, and x-ray Thomson scattering to diagnose these plasmas. He is now analyzing data and working on papers reporting the results. A paper on the x-ray Thomson scattering is nearing submission. Tony also participated in some measurements to understand spectrometer behavior with short laser pulses, which led to a publication.[27]

Graduate student **Channing Huntington** was asked to further advance x-ray Thomson scattering techniques, and has been developing methods to enable us to more distinctly determine the spatial profiles of temperatures and ionization in the radiative shocks with Xe gas. He performed some experiments on Omega in 2009 and 2010 and will again be shooting in April 2011. In 2010 he demonstrated techniques that will be used this year to measure temperatures at known locations relative to the primary shock. Chan, with graduate student **Christine Krauland**, also developed and published[28] an analysis of imaging x-ray scattering as a diagnostic technique. We have very high hopes for this technique in the NIF context. It remains to be seen whether we can get enough x-rays from Omega to make it effective there. Chan also did some experiments on the high-intensity HERCULES laser at Michigan, in collaboration with Karl Krushelnick's group. His resulting paper has been accepted by Physical Review Letters.[29] Several of our students have participated in our ongoing experiments on NIF, Chan authored a paper reporting our development of a backlit-pinhole diagnostic for these experiments.[30] Christine developed an experimental design for an experiment that we believe to have produced a radiative reverse shock last August. This experiment is relevant to the observed "hot spots" in cataclysmic variable stars. In June 2011 Christine will shoot an iterated version of this experiment. This is developing nicely into a novel direction for future research. Second-year graduate student **Rachel Young**, who has an interest in design, has worked with Eric Myra to learn to use the CRASH code, and will be using it to contribute multi-dimensional modeling of these experiments.

Graduate student **Eliseo Gamboa** has a significant interest in instrumentation. We have teamed him with David Montgomery at LANL to develop and use an imaging x-ray spectrometer for imaging x-ray Thomson spectroscopy. His ultimate goal is to develop a system that can effectively be fielded through a single diagnostic inserter (TIM) on Omega. This will enable one to obtain well-resolved spatial profiles of temperature and ionization, and will be useful to a very wide range of experiments in addition to our work with radiative shocks. Eliseo more recently has designed the imaging x-ray spectrometer, using a toroidal crystal, that can fit within a TIM on Omega. He has a paper discussing

the properties of such spectrometers ready for submission. LANL is building the first copy of the instrument Eliseo designed, for use in joint experiments. Eliseo has also participated in two experiments on the Trident laser facility at LANL. Eliseo's initial graduate student project involved the completion of a system for directly measuring the charge bunches produced by microchannel plates. This system will allow a more definite understanding of the noise properties of x-ray images produced using microchannel-plate intensifiers. He published a paper in Reviews of Scientific Instruments reporting his results.[31] This continues our long-term exploration of these devices, which previously led to a publications by Eric Harding[32] on optical pulse height measurements and modeling and by an undergraduate student[33] on the use of transmission photocathodes with them.

Our nonlinear hydrodynamics thrust has included work on instabilities driven by blast waves like those produced when supernovae explode, and work to observe the Kelvin-Helmholtz instability[34,35] under high-energy density conditions. We have previously published results of a sequence of experiments in which the initial conditions for the blast-wave-driven instabilities were varied, in an experiment scaled to the explosion dynamics of a well-known supernova (SN 1987A). These experiments[36,37] and related simulations[38-40] showed that some of our preconceptions about the impact of varying the initial conditions were not correct. We also observed that the morphology of the spikes of dense material penetrating the less-dense material has a number of mysterious features.[10] These mysterious features are potentially related to magnetic-field generation within these targets,[41] among other possibilities. In work going on now, graduate student **Carlos DiStefano** is experimentally investigating these features both by varying the target properties and by doing experiments that can detect magnetic fields if they are present. In a related effort, we developed and published[42] a design for a NIF experiment on blast-wave-driven instabilities, in which it will be possible to use a diverging system with two interfaces, with the masses of various layers scaled to those in the pre-supernova star. NIF shots based on this design have been approved.

VII. References

1 T.R. Boehly, R.S. Craxton, T.H. Hinterman, J.H. Kelly, T.J. Kessler, S.A. Kumpman, S.A. Letzring, R.L. McCrory, S.F.B. Morse, W. Seka, S. Skupsky, J.M. Soures, and C.P. Verdon, The upgrade to the OMEGA laser system, Rev. Sci. Intsr. 66, 508 (1995).

2 J.P. Holloway, D. Bingham, C.C. Chou, F.W. Doss, R.P. Drake, B. Fryxell, M.J. Grosskopf, B. van der Holst, B. Mallick, R.G. McClarren, A. Mukherjee, V. Nair, K.G. Powell, D. Ryu, I. Sokolov, G. Toth, and Z. Zhang, Predictive Modeling of a Radiative Shock System, Reliability Engineering and System Safety, doi:10.1016/j.ress.2010.08.011 (2011).

3 R.G. McClarren, D. Ryu, R.P. Drake, M.J. Grosskopf, D. Bingham, C.C. Chou, B. Fryxell, B. van der Holst, J.P. Holloway, C.C. Kuranz, B. Mallick, E. Rutter, and B.R. Torralva, A Physics Informed Emulator for Laser-Driven Radiating Shock Simulations, Reliability Engineering and System Safety, doi:10.1016/j.ress.2010.08.011 (2011).

[4] Pritam Ranjan, Derek Bingham Wilson Lu, Shane Reese, Brian J. Williams, Chuan-Chih Chou, Forrest Doss, Michael Grosskopf, and James Paul Holloway, Follow- up Experimental Designs for Computer Models and Physical Processes, Journal of Statistical Theory and Practice 5, 119 (2011).

[5] H.F. Stripling, R.G. McClarren, C.C. Kuranz, and M. J. Grosskopf, Calibration of uncertain inputs to computer models using experimentally measured quantiles and the BMARS emulator, International Conference on Mathematics and Computational Methods Applied to Nuclear Science and Engineering, 2011 American Nuclear Society.

[6] B. van der Holst, G. Toth, I.V. Sokolov, K. G. Powell, J. P. Holloway, E.S. Myra, Q. Stout, M.L. Adams, J. E. Morel, and R. P. Drake, A BLOCK-ADAPTIVE-MESH CODE FOR RADIATIVE SHOCK HYDRODYNAMICS: IMPLEMENTATION AND VERIFICATION, Astrophysical Journal Supplement Series 194, 23 (2011).

[7] R.G. McClarren, R. P. Drake, M.L. Adams, J. E. Morel, and J. P. Holloway, Theory of radiative shocks in the mixed, optically thick-thin case, Physics of Plasmas 17, 093301 (2010).

[8] R.G. McClarren and R. P. Drake, Radiative Transfer In the Cooling Layer of a Radiating Shock, Journal of Quantitative Spectroscopy and Radiative Transfer 111, 2095 (2010).

[9] F.W. Doss, H.F. Robey, R.P. Drake, and C.C. Kuranz, Wall shocks in high-energy-density shock tube experiments, Physics Of Plasmas 16, 112705 (2009).

[10] F.W. Doss, R.P. Drake, and C.C. Kuranz, Repeatability in radiative shock tube experiments, High Energy Density Physics 6, 157 (2010).

[11] F.W. Doss, C. C. Kuranz, and R. P. Drake, Statistical inference in the presence of an inclination effect in laboratory radiative shock experiments, Astrophysics and Space Science, submitted (2010).

[12] F.W. Doss, R.P. Drake, and E.S. Myra, Oblique radiative shocks, including their interactions with non-radiative polytropic shocks, Physics of Plasmas 18, 056901 (2011).

[13] R.G. McClarren and D. Holladay, Electron-Ion-Radiation Coupling Benchmarks For Verification of HEDP/IFE Codes, Fusion Science and Technology, in press (2011).

[14] J.T. Larsen and S.M. Lane, HYADES: a plasma hydrodynamics code for dense plasma studies, J. Quant. Spectrosc. Radiat. Transfer 51, 179 (1994).

[15] A.D.M. Walker, Radio Science Bulletin (2008).

[16] R.P. Drake, High Energy Density Physics: Fundamentals, Inertial Fusion and Experimental Astrophysics. (Springer Verlag, 2006).

[17] I. Benkevitch, I. V. Sokolov, D. Oberoi, and T. Zurbuchen, Ray Tracing in the Space Weather Modeling Framework, in preparation (2011).

[18] V.L. Ginzburg, The Propagation of Electromagnetic Waves in Plasmas. (Pergamon Press, 1964).

[19] A.B. Reighard, R. P. Drake, K.K. Dannenberg, D. J. Kremer, E.C. Harding, D.R. Leibrandt, S.G. Glendinning, T.S. Perry, B.A. Remington, J. Greenough, J. Knauer, T. Boehly, S. Bouquet, L. Boireau, M. Koenig, and T. Vinci, Collapsing radiative shocks in xenon on the Omega laser, Phys. Plas. 13, 082901 (2006).

[20] A.B. Reighard, R.P. Drake, T. Donjakowski, M.J. Grosskopf, K.K. Dannenberg, D. Froula, S. Glenzer, J.S. Ross, and J. Edwards, Thomson Scattering from a shock front, Rev. Sci. Inst. 77, 10E504 1 (2006).

[21] A.B. Reighard, R. P. Drake, J.E. Mucino, J.P. Knauer, and M. Busquet, Planar radiative shock experiments and their comparison to simulations, Phys. Plas. 14, 056504 (2007).

[22] A.B. Reighard and R.P. Drake, The formation of a cooling layer in a partially optically thick shock, Astrophysics and Space Science 307, 121 (2007).

[23] R. P. Drake and A. B. Reighard, Theory and experiment on radiative shocks, Shock Compression of Condensed Matter, AIP Conference Proceedings 845, 1417 (2006).

[24] R.P. Drake, Theory of radiative shocks in optically thick media, Phys. Plasmas 14, 043301 (2007).

[25] R.P. Drake, Energy balance and structural regimes of radiative shocks in optically thick media, IEEE Transactions on Plasma Science 35, 171 (2007).

[26] F.W. Doss, R.P. Drake, and H.F. Robey, Early-time stability of decelerating shocks, Astrophysical Journal, submitted (2009).

[27] A. Visco, R.P. Drake, D.H. Froula, S.H. Glenzer, and B.B. Pollock, Temporal dispersion of a spectrometer, Review Of Scientific Instruments 79, 10F545 (2008).

[28] C.M. Huntington, C.C. Krauland, C. C. Kuranz, S.H. Glenzer, and R. P. Drake, Imaging Scattered X-Ray Radiation for Measurement of Local Electron Density in High-Energy-Density Experiments, High Energy Density Physics, in press (2010).

[29] C. M. Huntington, A. G. R. Thomas, C. McGuffey, T. Matsuoka, V. Chvykov, G. Kalintchenko, S. Kneip, Z. Najmudin, C. Palmer, V. Yanovsky, A. Maksimchuk, R. P. Drake, T. Katsouleas, and K. Krushelnick, Current Filamentation Instability in Laser Wakefeld Accelerators, Physical Review Letters 106, 105001 (2011).

[30] C.M. Huntington, C.M. Krauland, C.C. Kuranz, R.P. Drake, H.-S. Park, D.H. Kalantar, A.G. MacPhee, B.A. Remington, and J. Kline, Short-duration backlit pinhole radiography diagnostics on the National Ignition Facility, Rev. Sci. Inst. 81, 10E536 (2010).

[31] E. J. Gamboa, C. M. Huntington, E. C. Harding, and R. P. Drake, Electronic measurement of microchannel plate pulse height distributions, Rev. Sci. Inst. 81, 10E310 (2010).

[32] E.C. Harding and R.P. Drake, A 3D model of x-ray induced microchannel plate output, Rev. Sci. Inst. 77, 10E312 1 (2006).

[33] M.E. Lowenstern, E.C. Harding, C. Huntington, A.J. Visco, and R.P. Drake, Performance of Au Transmission Photocathode on a Microchannel Plate Detector, Review Of Scientific Instruments 79, 10E912 (2008).

[34] E. C. Harding, J. F. Hansen, O. A. Hurricane, R. P. Drake, H. F. Robey, C. C. Kuranz, B. A. Remington, M. J. Bono, M. J. Grosskopf, and R. S. Gillespie, Observation of a Kelvin-Helmholtz Instability in a High-Energy-Density Plasma on the Omega Laser, Physical Review Letters 103 (2009).

[35] E. C. Harding, R. P. Drake, R. S. Gillespie, M. J. Grosskopf, A. Visco, J. Ditmar, Y. Aglitskiy, J.L. Weaver, and A. L. Velikovich, Laser driven supersonic flow

over a compressible foam surface on the Nike laser, Physics Of Plasmas, in press (2010).

[36] C.C. Kuranz, R.P. Drake, E.C. Harding, M.J. Grosskopf, H. F. Robey, B.A. Remington, M.J. Edwards, A.R. Miles, T.S. Perry, T. Plewa, N.C. Hearn, J.P. Knauer, D. Arnett, and D.R. Leibrandt, Two-dimensional blast-wave-driven Rayleigh-Taylor instability: experiment and simulation, Astrophysical Journal 696, 749 (2009).

[37] C.C. Kuranz, R.P. Drake, M.J. Grosskopf, A. Budde, C. Krauland, D.C. Marion, A.J. Visco, J.R. Ditmar, H. F. Robey, B.A. Remington, A.R. Miles, A.B.R. Cooper, C. Sorce, T. Plewa, N.C. Hearn, K.L. Killibrew, J.P. Knauer, D. Arnett, and T. Donajkowski, Three-dimensional blast-wave-driven Rayleigh-Taylor instability and the effects of long-wavelength modes, Physics Of Plasmas 16, 156310 (2009).

[38] N. Hearn, T. Plewa, R.P. Drake, and C.C. Kuranz, FLASH code simulations of Rayleigh-Taylor and Richtmyer-Meshkov instabilities in laser-driven experiments, Astrophysics and Space Science 307, 227 (2007).

[39] N.C. Hearn, T. Plewa, R.P. Drake, and C.C. Kuranz, Flash code simulations of laser-driven Rayleigh-Taylor and Richtmyer-Meshkov Experiments on Omega, in Proceedings of the Tenth International Workshop on The Physics of Compressible Turbulent Mixing, edited by M. Legrand and M. Vandenboomgaerde (Commissariat a l'Energie Atomique, Bruyeres-le-Chatel, 2007), pp. 114.

[40] A. Budde, R. P. Drake, C. C. Kuranz, M.J. Grosskopf, T. Plewa, and N.C. Hearn, Simulation of fabrication variations in supernova hydrodynamics experiments, High Energy Density Physics 6, 135 (2010).

[41] B. Fryxell, C. C. Kuranz, R. P. Drake, M.J. Grosskopf, A. Budde, T. Plewa, J. F. Hansen, A. R. Miles, and J. Knauer, The Possible Effects of Magnetic Fields on Laser Experiments of Rayleigh-Taylor Instabilities, High Energy Density Physics, in press (2010).

[42] M. J. Grosskopf, R. P. Drake, C. C. Kuranz, A. R. Miles, J. F. Hansen, T. Plewa, N. Hearn, D. Arnett, and J. C. Wheeler, Modeling of multi-interface, diverging, hydrodynamic experiments for the National Ignition Facility, Astrophysics and Space Science 322, 57 (2009).